All-sky search for gravitational wave emission from scalar boson clouds around spinning black holes in LIGO O3 data

R. Abbott *et al.*[*]
(The LIGO Scientific Collaboration, the Virgo Collaboration, and the KAGRA Collaboration)

(Received 30 November 2021; accepted 13 April 2022; published 9 May 2022)

This paper describes the first all-sky search for long-duration, quasimonochromatic gravitational-wave signals emitted by ultralight scalar boson clouds around spinning black holes using data from the third observing run of Advanced LIGO. We analyze the frequency range from 20 to 610 Hz, over a small frequency derivative range around zero, and use multiple frequency resolutions to be robust towards possible signal frequency wanderings. Outliers from this search are followed up using two different methods, one more suitable for nearly monochromatic signals, and the other more robust towards frequency fluctuations. We do not find any evidence for such signals and set upper limits on the signal strain amplitude, the most stringent being $\approx 10^{-25}$ at around 130 Hz. We interpret these upper limits as both an "exclusion region" in the boson mass/black hole mass plane and the maximum detectable distance for a given boson mass, based on an assumption of the age of the black hole/boson cloud system.

DOI: 10.1103/PhysRevD.105.102001

I. INTRODUCTION

Theories of beyond standard model physics allow for the production of ultralight bosons that could constitute a portion or all of dark matter [1–6]. If such ultralight bosons exist, they could appear around rotating black holes due to quantum fluctuations [7]. They would then scatter off and extract angular momentum from these black holes, and form macroscopic clouds, i.e. boson condensates, through a superradiance process [7,8]. The energy structure of the clouds resembles that of a hydrogen atom, earning boson clouds the name "gravitational atoms" in the sky. After the black hole spin decreases below a threshold, the superradiance process stops and the cloud depletes over time mainly through the annihilation of bosons into gravitons, which generates quasimonochromatic, long-duration gravitational waves when the self-interaction for bosons is weak.

The signal would also have a small, positive frequency variation, known as a "spin-up," that would arise from the classical contraction of the cloud over time as it loses mass [7]. The values of the spin-up depend on whether we consider scalar [9], vector [10,11], or tensor [12] boson clouds, but in this search we consider scalar boson cloud signals with very small spin-ups, of maximum $\mathcal{O}(10^{-12})$ Hz/s. Recently, the effect on gravitational-wave emission from boson self-interactions has been studied for the scalar case [13], showing that the signal can be significantly affected, including the magnitude of the spin-up, as the self-interaction increases.

The gravitational-wave signal frequency depends primarily on the mass of the boson, and weakly on the mass and spin of the black hole. Recently, exclusion regions of the black hole/scalar boson mass parameter space were calculated using upper limits from an all-sky search for spinning neutron stars in LIGO/Virgo data from the second observing run (O2) [14]. Furthermore, a search for boson clouds from Cygnus X-1 was performed with a hidden Markov model (HMM) method [15] on the same dataset, and disfavored particular boson masses for this object [16]. It has been suggested [17] that current methods for all-sky searches, such as the one used in [14], could suffer a significant sensitivity penalty in the extreme case of a population of 10^8 black holes in the Milky Way, due to the superposition of many signals in a small frequency range (as a consequence of the signal's frequency dependence at leading order on the boson mass). A detailed study [18] has quantified this effect, showing that the actual average loss of sensitivity is at most of about 15% for a signal "density" of 1–3 signals per frequency bin, while it rapidly reduces, and becomes negligible, for both lower and higher densities.

In addition to quasimonochromatic gravitational waves emitted by boson clouds around isolated black holes, it is also possible to probe the existence of boson clouds in binary black hole coalescences. One avenue requires measurements of spin: in principle, boson clouds will extract mass and spin from black holes, resulting in low spin values for black holes compared to those in a universe without boson clouds; in practice, individual black hole spins are hard to measure [19,20], and the current spin distribution of black holes depends on both the mass of

[*]Full author list given at the end of the article.

boson clouds and the distribution of spins when the black holes were born [21,22]. It is therefore interesting to combine spin measurements from various black hole mergers, via hierarchical Bayesian inference, to obtain constraints on boson cloud/spin interactions [23,24]. Additionally, the presence of a boson cloud will induce a change in the waveforms used in compact binary searches, e.g. new multipole moments and tidal effects (parametrized as Love numbers) [25,26], and such differences in binary black hole mergers may actually be detectable depending on the boson mass and field strength [27]. It has also been proposed to combine multiband observations of black hole mergers and boson cloud signals when future detectors are online [28], and to search for a stochastic gravitational-wave background from scalar and vector boson cloud signals [29–32]. Complementary methods [33,34] and searches [35,36] for ultralight scalar and vector bosons have also been developed that use the gravitational-wave interferometers as particle detectors, which provide additional constraints on the boson mass. Ultralight bosons can therefore have different effects on different types of gravitational-wave signals.

This paper presents results from the first all-sky search tailored to gravitational waves from depleting scalar boson clouds around black holes using the Advanced LIGO [37] data in the third observing run (O3). Although the expected gravitational-wave signal is almost monochromatic, it could come from anywhere in the sky; thus, the Doppler modulations from the relative motion of the Earth and the source, of $\mathcal{O}(10^{-4}f)$, where f is the frequency of the signal, are *a priori* unknown. A fully coherent search, in which we take a single Fourier transform of the whole data set and look for peaks in the power spectrum after demodulating the data, is therefore impossible to perform in each sky direction because of limited computational power. Indeed, the number of sky positions to search over scales with the square of both the Fourier transform length and the frequency, and would amount to $\mathcal{O}(10^{20})$ at high frequencies [38]. This means that we must employ semicoherent methods, in which we break the data into smaller chunks in time that are analyzed coherently, and then combined incoherently, to keep the computational cost under control while retaining the desired sensitivity [39–41]. Moreover, we adopt a multiresolution approach, equivalent to considering several different Fourier transform lengths [42], in order to be sensitive towards possible unpredicted frequency fluctuations of the gravitational-wave signal.

This paper is organized as follows: in Sec. II, we describe our model for a gravitational-wave signal resulting from a depleting scalar boson cloud around a rotating black hole; in Sec. III, we explain our method to search for such signals; in Sec. IV, we provide information on the datasets we use in our analysis; in Sec. V, we present the results of the search and our upper limits, including their astrophysical interpretations in terms of constraints in the boson/black hole mass plane and on the maximum detectable distance; finally, in Sec. VI, we discuss prospects for future work. Appendices contain details on the follow-up of selected outliers.

II. THE SIGNAL

An isolated black hole is born with a defining mass, spin and charge [43]. Ultralight boson particles around a black hole will scatter off it and extract energy and momentum from it if the so-called *superradiant* condition is satisfied, i.e. $\omega < m\Omega$ [7,44] where ω is the angular frequency of the boson (related to the boson mass linearly), m is the azimuthal quantum number in the hydrogenlike gravitational atom, and Ω is the angular frequency of the rotating black hole's outer horizon. Because the bosons have a finite mass, they become gravitationally bound to the black hole, which allows for successive scatterings and a build-up of a macroscopic cloud, extracting up to about 10% of the black hole mass [7]. This process is maximized when the particle's reduced Compton wavelength is comparable to the black hole radius:

$$\frac{\hbar c}{m_b} \simeq \frac{GM_{\rm BH}}{c^2}, \tag{1}$$

where m_b is the boson mass-energy, $M_{\rm BH}$ is the black hole mass, $\hbar$ is the reduced Planck's constant, and c is the speed of light. The typical time scale of the superradiance phase is [9]

$$\tau_{\rm inst} \approx 27\left(\frac{M_{\rm BH}}{10\ M_\odot}\right)\left(\frac{\alpha}{0.1}\right)^{-9}\left(\frac{1}{\chi_i}\right)\ \text{days}, \tag{2}$$

where χ_i is the black hole initial dimensionless spin, and

$$\alpha = \frac{GM_{\rm BH}}{c^3}\frac{m_b}{\hbar} \tag{3}$$

is the fine-structure constant in the gravitational atom.

Once the superradiant condition is no longer satisfied, the growth stops, and the cloud begins to give off energy primarily via annihilation of particles in the form of gravitational waves [15], over a typically much longer timescale which, for $m = 1$ and in the limit $\alpha \ll 0.1$, is given by

$$\tau_{\rm gw} \approx 6.5 \times 10^4\left(\frac{M_{\rm BH}}{10\ M_\odot}\right)\left(\frac{\alpha}{0.1}\right)^{-15}\left(\frac{1}{\chi_i}\right)\ \text{years}. \tag{4}$$

For scalar bosons, these clouds have a much shorter growth timescale compared to the timescale for them to deplete [9]; thus, if they exist now, they are more likely to be depleting rather than growing. The gravitational-wave emission is at a frequency $f_{\rm gw}$ [14]:

$$f_{\rm gw} \simeq 483\ {\rm Hz}\left(\frac{m_{\rm b}}{10^{-12}\ {\rm eV}}\right) \times \left[1 - 7\times 10^{-4}\left(\frac{M_{\rm BH}}{10\ M_\odot}\frac{m_{\rm b}}{10^{-12}\ {\rm eV}}\right)^2\right]. \quad (5)$$

In fact, this frequency slowly increases in time due to the cloud self-gravity and particle self-interaction, quantified by the boson self-interaction constant F_b [13]. As in [13], we consider a scalar boson that, in addition to a nonzero mass, has a quartic interaction with an extremely small coupling λ, and characterize this coupling in terms of the parameter $F_b \coloneqq m_b/\sqrt{\lambda}$. In the context of an axionlike particle, F_b would roughly correspond to the symmetry breaking energy scale.

Specifically, if $F_b \gtrsim 2\times 10^{18}$ GeV, the spin-up is dominated by the cloud self-gravity and is given by

$$\dot{f}_{\rm gw} \approx 7\times 10^{-15}\left(\frac{m_{\rm b}}{10^{-12}\ {\rm eV}}\right)^2\left(\frac{\alpha}{0.1}\right)^{17}\ {\rm Hz/s}. \quad (6)$$

With this condition on F_b, our search probes energies at the Planck scale, and is sensitive to the QCD axion with a mass of $\sim 10^{-13}$–10^{-12} eV [13]. However, for smaller F_b a spin-up term, due to the cloud self-gravity and change of the black hole mass, of the form

$$\dot{f} \approx 10^{-10}\left(\frac{m_{\rm b}}{10^{-12}\ {\rm eV}}\right)^2\left(\frac{\alpha}{0.1}\right)^{17}\left(\frac{10^{17}\ {\rm GeV}}{F_b}\right)^4\ {\rm Hz/s} \quad (7)$$

is dominant in the intermediate self-interaction regime, for $8.5\times 10^{16}(\alpha/0.1)\ {\rm GeV} \lesssim F_b \lesssim 2\times 10^{18}$ GeV (a term with a similar scaling appears due to energy level transitions). In this regime, the signal duration significantly shortens, thus reducing the chance of detection. In the strong self-interaction regime, when $F_b \lesssim 8.5\times 10^{16}(\alpha/0.1)$ GeV, the spin-up can be parametrized as

$$\dot{f} \approx 10^{-10}\left(\frac{m_{\rm b}}{10^{-12}\ {\rm eV}}\right)^2\left(\frac{\alpha}{0.1}\right)^{17}\left(\frac{10^{17}\ {\rm GeV}}{F_b}\right)^6\ {\rm Hz/s}, \quad (8)$$

and the signal strength rapidly decreases with increasing interaction, making the detection of annihilation signals basically impossible for current detectors. In Sec. V C, we will briefly discuss the implication of our search results in relation to the value of F_b. Moreover, at the analysis level we do not want to exclude the possibility that the emitted signal frequency evolves in a more complicated manner than we model, e.g. there are random fluctuations. In Sec. III D, we describe a computationally cheap method to deal with such frequency variations.

The signal we are considering have lower amplitudes than those from compact binary coalescences [17], with initial values (for $\alpha \ll 0.1$)

$$h_0 \approx 6\times 10^{-24}\left(\frac{M_{\rm BH}}{10\ M_\odot}\right)\left(\frac{\alpha}{0.1}\right)^7\left(\frac{1\ {\rm kpc}}{D}\right)(\chi_i - \chi_c), \quad (9)$$

where

$$\chi_c \approx \frac{4\alpha}{4\alpha^2+1}, \quad (10)$$

is the black hole spin when the superradiance is saturated, and D is the source distance. The emitted signal amplitude decreases in time as the clouds are depleted, according to

$$h(t) = \frac{h_0}{1+\frac{t}{\tau_{\rm gw}}}. \quad (11)$$

The equations above are analytic approximations to the true behavior of a gravitational wave originating from boson clouds. When we consider $\alpha \sim 0.1$, we must account for the difference between the numerical and analytic solutions, which is ~3 in energy at the highest α considered here, $\alpha \sim 0.15$ We obtain this factor of ~3 comparing the black and red curves in Fig. 2 of [9] at $\alpha \sim 0.15$.

III. SEARCH METHOD

The semi-coherent method we employ is based on the band sampled data (BSD) framework [45], which is being used in an increasing number of continuous-wave searches, due to its flexibility and computational efficiency [46–48]. BSD files are data structures that store a reduced analytic strain-calibrated time series in 10-Hz/one-month chunks. To construct BSD files, we take a Fourier transform of a chunk of time-series strain data, extract a 10-Hz band, keep only the positive frequency components, and inverse Fourier transform to obtain the reduced analytic signal.

The main steps of the analysis pipeline are schematically shown in Fig. 1 and are summarized below.

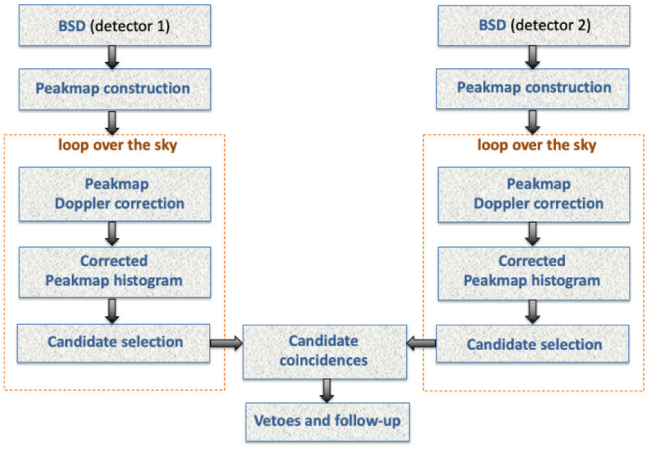

FIG. 1. Scheme of the search pipeline.

A. Peakmap construction

Our analysis starts with a set of BSD files covering the whole third observing run and frequencies between 20 and 610 Hz. The maximum frequency is chosen to ensure the computational cost of the analysis is reasonable, and is consistent with the fact that the most relevant part of the accessible parameter space of the black hole-boson system corresponds to the intermediate frequencies. Each of these time series is divided into chunks of duration

$$T_{\mathrm{FFT}} = \frac{1}{\Omega_{\mathrm{rot}}}\sqrt{\frac{c}{2f_{10}R_{\mathrm{rot}}}}, \tag{12}$$

where f_{10} is the maximum frequency of each corresponding 10-Hz band, $\Omega_{\mathrm{rot}} = 2\pi/86164.09$ rad/s is the Earth sidereal angular frequency, and R_{rot} is the Earth rotational radius, which we conservatively take as that corresponding to the detector at the lowest latitude ($R_{\mathrm{rot}} = 5.5 \times 10^6$ km for the Livingston detector). This T_{FFT} length guarantees that, if we take the Fourier transform of the chunk, the power spread of any possible continuous-wave signal, caused by the motion of the Earth with respect to the source, is fully contained in one frequency bin with a width of $\delta f = 1/T_{\mathrm{FFT}}$ in each chunk. In Fig. 2, the chunk duration is shown as a function of the frequency. For each of these chunks, with at least a 50% of nonzero values, the square modulus of the Fourier transform is computed (by means of the FFT algorithm) and divided by an estimation of the average spectrum over the same time window. The resulting quantity has a mean value of one independently of the frequency—for this reason it is called the *equalized* spectrum—and takes values significantly different from one when narrow frequency features are present in the data. We select prominent peaks in the equalized spectra, defined as time-frequency pairs that correspond to local maxima and have a magnitude above a threshold of $\theta = 2.5$ [38]. The collection of the these time-frequency peaks forms the so-called *peakmap*, see e.g. [38] for more details.

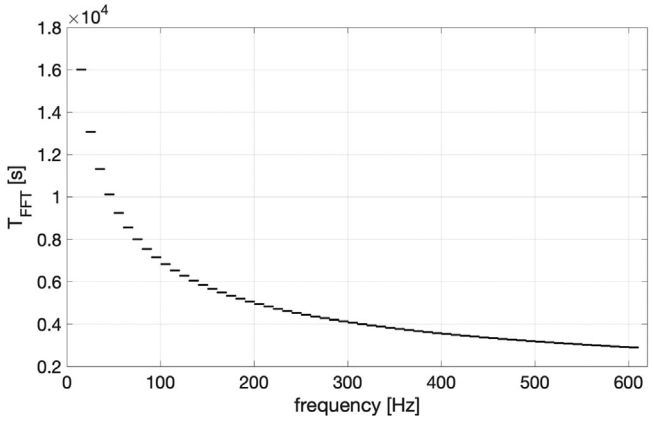

FIG. 2. Chunk duration T_{FFT} as a function of frequency. The T_{FFT} is fixed within each 10-Hz band.

B. Doppler effect correction

We build a suitable grid in the sky such that, after the Doppler effect correction for a given sky direction, any residual Doppler effect always produces an error in frequency within half a frequency bin [38]. For each sky direction in the grid, the peaks in the peakmap are shifted in order to compensate for the time-dependent Doppler modulation, according to the relation

$$f_{0,\mathrm{t_k}} = \frac{f_{\mathrm{obs,t_k}}}{1 + \frac{\vec{v}_{\mathrm{t_k}}\cdot\hat{n}}{c}}, \tag{13}$$

where $f_{\mathrm{obs,t_k}}$ is an observed frequency peak at the time t_k, $\vec{v}_{\mathrm{t_k}}$ is the detector's velocity, and $\hat{n}$ is the unit vector identifying the sky direction.

As we have described in Sec. II, the signal has an intrinsic spin-up, associated with the cloud depletion. Although we do not apply an explicit correction for the spin-up, the analysis retains most of the signal power—with a maximum sensitivity loss less than a few percent[1]—as long as the corresponding frequency variation during the full observation time T_{obs} is confined within $\pm 1/2$ bin of the frequency evolution rate $\delta\dot{f}$, given by

$$\delta\dot{f} = \frac{1}{2T_{\mathrm{obs}}T_{\mathrm{FFT}}}. \tag{14}$$

The $\delta\dot{f}$ value is plotted as a function of the frequency in Fig. 3.

C. Peakmap projection

Once we have applied the Doppler correction, we project the peakmap onto the frequency axis and select the most significant frequencies for further analysis. Indeed, if a monochromatic signal comes from a given direction, we expect its associated peaks to be aligned in frequency and appear as a prominent peak in the projected peakmap, when the signal is strong enough. The statistics of the peakmap are described in detail in [38], so here we only provide a brief review. In the absence of signals, the probability p_0 of selecting a peak depends on the noise distribution. In the case of Gaussian noise, it is given by

$$p_0 = e^{-\theta} - e^{-2\theta} + \frac{1}{3}e^{-3\theta}, \tag{15}$$

[1]In principle, the maximum sensitivity loss would be of about 36%, when the corrected signal frequency falls in the middle among two consecutive frequency bins. In practice, however, the application of the moving average on the peakmaps, see Sec. III D, allows us to recover part of the lost signal power, reducing the maximum loss to about 19% (when applying a moving average of two bins, i.e. a window with $W = 2$).

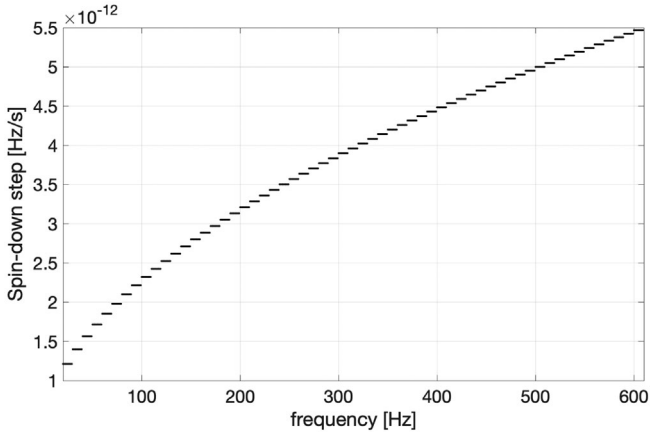

FIG. 3. Bin size of the frequency time derivative, $\delta\dot{f}$, a function of the frequency, given the full observing time of O3 and T_{FFT} chosen for each 10-Hz band. The search by default covers a frequency time derivative range of $\dot{f} \in [-\delta\dot{f}/2, \delta\dot{f}/2]$. Such a range contributes to set constraints on the portion of the boson mass/black hole mass explored in the search.

where $\theta = 2.5$ is the threshold we apply to construct the peakmap. On the other hand, if a signal with spectral amplitude (in units of equalized noise)

$$\lambda = \frac{4|\tilde{h}(f)|^2}{T_{\mathrm{FFT}} S_n(f)}, \tag{16}$$

where $\tilde{h}(f)$ is the signal Fourier transform, and $S_n(f)$ is the detector noise power spectral density, is present, the corresponding probability p_λ of selecting a signal peak, for weak signals with respect to the noise level, is given by

$$p_\lambda = p_0 + \frac{\lambda}{2}\theta(e^{-\theta} - 2e^{-2\theta} + e^{-3\theta}). \tag{17}$$

The statistic of the peakmap projection is, for well-behaved noise, a binomial with expectation value $\mu = Np_0$, where N is the number of FFTs, and standard deviation $\sigma = \sqrt{Np_0(1-p_0)}$. In the presence of a signal, the expected number of peaks at the signal frequency (after the Doppler correction) is Np_λ. It is then useful to introduce the critical ratio (CR):

$$\mathrm{CR} = \frac{n-\mu}{\sigma}, \tag{18}$$

where n is the actual number of peaks in a given frequency bin, which, in the limit of large N (in practice, greater than a ∼30), closely follows a Gaussian distribution with zero mean and unity standard deviation.

D. Peakmap moving averages

The signal emitted by a boson cloud is not exactly monochromatic, due to the presence of a spin-up, see Sec. II. Moreover, further unpredicted frequency fluctuations could be present, due to our limited knowledge of the physical processes actually taking place. A signal with varying frequency can be characterized by its *coherence time*, defined as the minimum amount of time over which the signal frequency variation exceeds the search frequency bin. For the sake of robustness, in order to deal with spin-up values which cause a frequency variation larger than half a frequency bin during the observing time T_{obs} (see Sec. III C) and—especially—to take into account possible uncertainties in the signal morphology, we apply a sequence of moving averages over a window width W varying from two to ten frequency bins, starting from the Doppler corrected peakmap projection. This procedure can be shown to be equivalent—and computationally much more efficient—to build peakmap projections with an equivalent FFT duration $\approx T_{\mathrm{FFT}}/W$. While these moving averages reduce the sensitivity to signals with a characteristic coherence time larger than T_{FFT}, e.g. purely monochromatic signals, they provide better sensitivity to signals with a typical coherence time comparable to the equivalent FFT duration [42]. At the same time, they allow us to partially recover sensitivity to spin-ups larger than those shown in Fig. 3.

E. Candidate selection and coincidences

We use the CR as a detection statistic to identify potentially interesting outliers. Outliers are uniformly selected in the parameter space by taking the two points with the highest CR in each peakmap projection, for each sky position in every 0.05-Hz frequency band, independent of the actual CR values, as long as it is above a minimum value of 3.8.

In the next step, we identify coincident pairs among outliers found in the Hanford and Livingston data, corresponding to the same W, by using a dimensionless coincidence window of 3. In other words, two outliers, one from Hanford and the other from Livingston, are considered coincident if the dimensionless distance

$$d = \sqrt{\left(\frac{\Delta f}{\delta f}\right)^2 + \left(\frac{\Delta\lambda}{\delta\lambda}\right)^2 + \left(\frac{\Delta\beta}{\delta\beta}\right)^2} \leq 3, \tag{19}$$

where $\Delta f, \Delta\lambda, \Delta\beta$ are the differences between parameter values of the outliers found in Hanford (H1) and Livingston (L1), and $\delta f, \delta\lambda, \delta\beta$ are the corresponding bin sizes.[2] The coincidence window of 3 is chosen according to the studies carried out using simulated signals and is consistent with the choice in standard all-sky searches for neutron stars [49,50].

[2]The sky position bin sizes in general are different for two outliers identified at different sky positions, so the average among the corresponding bin sizes is actually used.

F. Postprocessing

Coincident outliers are subject to a sequence of postprocessing steps in order to discard those incompatible with an astrophysical signal.

The first veto is to check if some of the outliers are compatible with known narrow-band instrumental disturbances, also known as *noise lines*. An outlier is considered as caused by a noise line, and thus discarded, if its Doppler band, defined by $\Delta f_{\mathrm{dopp}} = \pm 10^{-4} f$, where f is the outlier frequency, intersects the noise line.

The next is a consistency veto, in which a pair of coincident outliers are discarded if their CR is not compatible with the detectors' noise level at the corresponding frequency. Specifically, we veto those coincident outliers for which the CR in one detector is more than a factor of 5 different than that in the other detector, after being weighted by the detector's power spectral density [14,50]. This choice, also used in standard all-sky searches for continuous waves from neutron stars, is motivated by the desire to safely eliminate an outlier only if the discrepancy is really significant and the CR is large in at least one of the two detectors (i.e. a real astrophysical signal is not expected to behave that way).

The previous steps are all applied to coincident outliers separately for each value of the moving average window width W. In case of outliers coincident across different W values, only the one with the highest CR is kept.[3]

G. Follow-up

Outliers with $W = 1$, the case in which we do not apply moving averages, could be due to monochromatic signals or signals with very small fluctuations in frequency, while outliers with $W > 1$ are more compatible with signals characterized by a larger degree of frequency fluctuation. These two sets of candidates are then followed up with different methods, one based on the Frequency-Hough algorithm and used e.g. in [49], and the other using the Viterbi method, see e.g. [16]. Both methods are briefly explained in Appendix B.

IV. DATA

We use data collected by the Advanced LIGO gravitational-wave detectors over the O3 run, which lasted from April 1, 2019 to March 27, 2020, with a one-month break in data collection in October 2019. The duty cycles of the two detectors, H1 and L1, are ∼76% and ∼77%, respectively, during O3.

In the case of a detection, the calibration uncertainties in the detector strain data stream could impact the estimates of the boson properties. Without a detection, these uncertainties could affect the estimated instrument sensitivity and inferred upper limits on astrophysical source properties. The analysis uses the "C01" version of calibrated data,[4] which has estimated maximum uncertainties (68% confidence interval) of ∼7%–11% in magnitude and ∼4 deg–9 deg in phase, over the first/second halves of O3 [51,52]. The frequency-dependent uncertainties vary over the course of a run but do not change by large values. The time-dependent variations could lead to errors in opposite directions at a given frequency during different time periods. In addition, the calibration errors and uncertainties are different at the two LIGO sites. By integrating the data over the whole run, we expect that the impact from the time-dependent, frequency-dependent calibration uncertainties cancels out to some extent, and the overall impact on the inferred upper limits is within a level of ∼2%. Thus we do not explicitly consider the calibration uncertainties in our analysis.

Due to the presence of a large number of transient noise artifacts, a *gating* procedure [53,54] has also been applied to the LIGO data. This procedure applies an inverse Tukey window to the LIGO data at times when the root-mean-square value of the whitened strain channel in the band of 25–50 or 70–110 Hz exceeds a certain threshold. Only 0.4% and ∼1% of data is removed for Hanford and Livingston, respectively, and the improvement in data quality from applying such gating is significant, as seen in the stochastic and continuous gravitational-wave analyses in O3 [55].

V. RESULTS

In this section, we present the results of the analysis described in Sec. III. With no candidates surviving the follow-up, we present the upper limits on the signal strain amplitude in Sec. V B, and the astrophysical implications in Sec. V C.

Coincident outliers produced by the main search are first pruned in order to reduce their number to a manageable level. A further reduction is based on a close case-by-case inspection of the strongest outliers, as described in the following.

A. Outlier vetoes

First, we remove outliers due to *hardware injections*, which simulate the gravitational wave signals expected from spinning neutron stars, added for testing our analysis methods by physically moving the mirrors as if a signal had arrived. See Appendix A for more details.

Moreover, we find several bunches of outliers which are not compatible with astrophysical signals, and thus are also discarded and not followed up. In these cases, the

[3]This restriction reduces the computational cost with only a small loss in sensitivity.

[4]This is equivalent to the publicly available frame data titled "HOFT_CLEAN_SUB60HZ_C01_AR" at https://www.gw-openscience.org/O3/.

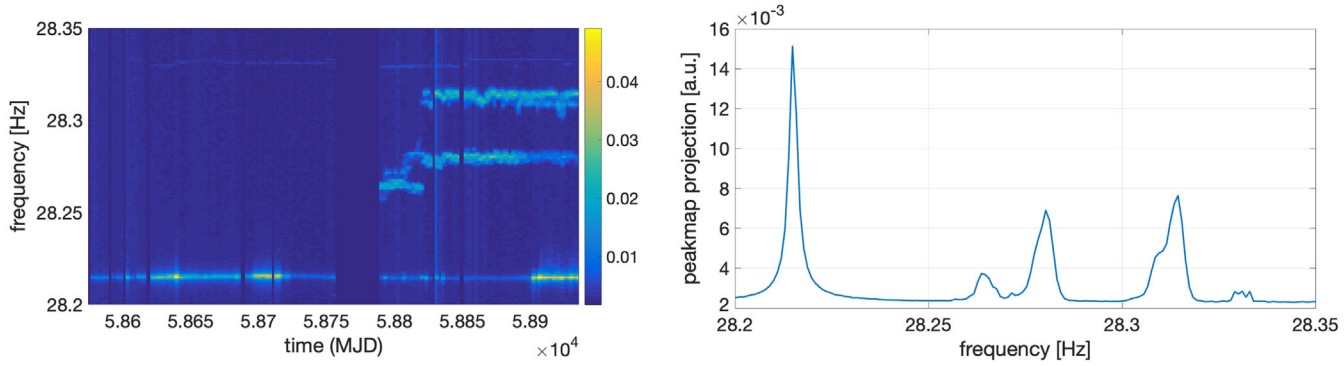

FIG. 4. Time-frequency peakmap (left) and corresponding projection (right) in the frequency band of 28.2–28.35 Hz over the full run. Several instrumental artifacts are visible, e.g. strong lines with varying amplitudes (∼28.22 Hz), weaker lines with sudden frequency variation (∼28.33 Hz), and broad transient disturbances (vertical bright lines). In particular, the features around 28.28 Hz in the second half of O3 are responsible for a big bunch of outliers with frequency in the range of 28.279–28.283 Hz.

time-frequency peakmaps and spectra show the presence of broadband disturbances or lines. Examples of such disturbances are shown in Fig. 4, where we plot on the left the time-frequency peakmap in the frequency range of 28.2–28.35 Hz over the whole run and on the right the corresponding projection onto the frequency axis. A wide and strong transient disturbance responsible for many outliers with frequency in the range of 28.279–28.283 Hz is clearly visible.

In addition, we find an excess of outliers at several multiples of 10 Hz in both H1 and L1 data, starting from 230 Hz. These are artifacts produced by the procedure to build BSDs.[5] As it is extremely unlikely that the real astrophysical signals are coincident with multiples of 10 Hz, we veto all candidates within a range of $\pm 10^{-4}$ Hz around each multiple of 10 Hz.

Finally, we apply a final threshold on the CR in order to further reduce the number of outliers to a small enough number to permit follow up. In particular, we use different thresholds $\mathrm{CR}_{\mathrm{thr}} = 4.1$ and 4.4 for outliers with $W = 1$ and $W > 1$, respectively. This procedure leaves us with 9449 outliers with $W = 1$ and 7816 outliers with $W > 1$. The choice of threshold does not affect the upper limits presented later, since those are based on the outliers with the highest CR.

Such outliers are followed-up with two different methods: a method based on the Frequency-Hough algorithm if the outliers are characterized by $W = 1$ (Appendix B 1), and a method based on a HMM tracking scheme (the Viterbi algorithm) if the outliers are characterized by $W > 1$ (Appendix B 2). No potential CW candidate remains after the follow-up. Details of the follow-up procedure and results are presented in Appendix C.

[5]The artifacts are a well-known consequence of the 10 Hz baseline used to build BSD files. They could be avoided by constructing the BSDs with interlaced frequency bands.

B. Upper limits

Having concluded that none of the outliers is compatible with an astrophysical signal, we compute 95% CL upper limits placed on the signal strain amplitude.

The limits are computed, for every 1-Hz sub-band in the range of 20–610 Hz, with the analytic formula of the Frequency-Hough sensitivity, given by Eq. (67) in [38], where the relevant quantities, i.e. an estimate of the noise power spectral density S_n and the CR, are obtained from the O3 data used in this search. Specifically, for each 1-Hz subband, we take the maximum CR of the outliers, separately for Hanford and Livingston detectors, and the detectors' averaged noise spectra in the same subband. We then compute the two 95% confidence-level upper limits using the equation, and take the worse (i.e. the higher) among the two.

This procedure has been validated by injecting simulated signals into LIGO and Virgo O2 and O3 data [56]. In particular, this procedure has been shown to produce conservative upper limits with respect to those obtained with a much more computationally demanding injection campaign. It has been also verified that the upper limits obtained with a classical procedure based on injections are always above those based on the same analytical formula but using the minimum CR in each 1-Hz subband. The two curves, based, respectively, on the highest and the smallest CR, define a belt containing both a more stringent upper limit estimation and the sensitivity estimation of our search. When we will discuss the astrophysical implications of the search, we will always refer to the upper limits obtained using Eq. (67) in [38], which are conservative with respect to limits derived from injections. This same procedure is being used for the O3 standard all-sky search for continuous waves from spinning neutron stars [57]. Equation (67) of [38] gives the minimum detectable amplitude at a given confidence level, and has been derived by marginalizing over sky position and polarization of the source.

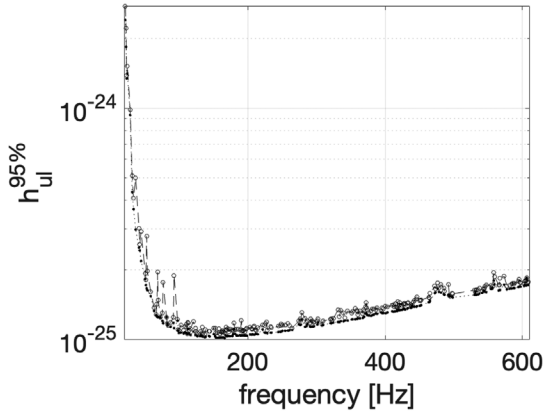

FIG. 5. 95% C.L. upper limits on the signal strain amplitude obtained from this search (circles, connected by the dashed line). Values are given in each 1-Hz subband. No value is given for the subbands where no outlier survives. The dots connected by a dashed line define the lower bound obtained using the minimum CR in each subband.

The resulting upper limits are shown in Fig. 5, as circles connected by a dashed line. The minimum value is 1.04×10^{-25} at 130.5 Hz. In the same figure, the dots connected by the dashed line correspond to the lower bound computed using the minimum CR. A comparison with previous all-sky searches, see e.g. Fig. 4 of [58] or Fig. 6 of [59], shows that our conservative results are better than most of the past searches, including the recent early O3 analysis [58]. In particular, our minimum upper limit value improves upon that in [58] by ∼30%. The main factors that contribute to the improvement relative to [58] are (1) the use of the full O3 C01 gated data, (2) the use of longer FFTs at least in a portion of the frequency band, and (3) the restricted spin-up/down range that could impact the maximum CR and thus the upper limit in each subband. On the other hand, the all-sky search described in [58], as well as most of the other past searches, cover a significantly larger parameter space in both the spin-down/up and frequency ranges, and thus are sensitive to signals that are not considered in this analysis. An O2 all-sky search reported in [60] produces upper limits slightly better than ours, by about 5–10% on average (due to the use of a much longer coherent integration time of days), but obtained over a smaller parameter space and more limited in scope, being focused on low-ellipticity sources. See Sec. VI for a more detailed discussion.

We want to stress two important points here. First, our conservative procedure to compute upper limits, based on the maximum CR in each subband, produces strain values that are typically larger than the minimum detectable amplitudes at the same frequency. That is, the search sensitivity is expected to be better than the upper limits. Second, this is the first all-sky search that is optimized for frequency wandering signals, both at the level of outlier selection and follow-up. This allows us to achieve a better sensitivity to such signals compared to that achievable using the maximum possible FFT duration (which is the best choice for nearly monochromatic signals).

C. Astrophysical implications

The upper limits presented above can be translated into physical constraints on the source properties. We interpret the results in two different ways. First, similar to what has been done in [14], we compute the exclusion regions in the boson mass and black hole mass plane, assuming fixed values of the other relevant parameters, namely the distance to the system D, the initial dimensionless spin of the black hole χ_i, and a time equal to the age of the cloud $t = t_{\rm age}$. Indeed, from Eqs. (9) and (11), once D, $\chi_{\rm i}$, and $t_{\rm age}$ are fixed, the signal strain amplitude depends only on the boson mass m_b and black hole mass $M_{\rm BH}$. Thus for each pair of $(m_b, M_{\rm BH})$, we can exclude the presence of a source with those assumed parameters, if it would have produced a signal whose strain is larger than the upper limit at a given frequency in Fig. 5. In our search, the α values probed roughly fall in the range of [0.02, 0.13]. Equations (4) and (9) do not hold in the range of $\alpha \gtrsim 0.1$, as shown in Fig. 2 of [9]. Specifically, we look at the Brito + curve derived analytically compared to the black curve obtained from numerical simulations, and see that they differ in energy by a factor of 3 at the largest α considered in this search, α 0.15. This implies that we underestimate $\tau_{\rm gw}$ up to a factor of 3 and overestimate h_0 up to a factor of $\sqrt{3}$ (at $\alpha \simeq 0.13$). Thus we correct Eqs. (4) and (9) by these factors such that the resulting exclusion regions are slightly conservative in the whole parameter space. In Fig. 6, the exclusion regions are plotted for $D = 1$ kpc (left) and $D =$ 15 kpc (right), assuming a high initial spin of $\chi_i = 0.9$. For each distance assumption, three different values of the black hole age are considered. In Fig. 7, the exclusion regions are shown for the same parameters as before, except that a lower initial spin value, $\chi_i = 0.5$ is assumed. In both cases, as expected, the constrained region is smaller when the source is assumed to be at a farther distance as, in this case, the signal amplitude at the detector is smaller. For any given black hole mass, these results improve upon the constraints obtained in Advanced LIGO O2 data [14] for lower boson masses, while they are slightly less constraining for higher boson masses. This is because for a given black hole mass, higher boson masses correspond to higher signal spin-up [see Eq. (6)], and we simply do not cover a large spin-up range. On the other hand, the constraints described in [14] were obtained from the results of a search not specifically designed for boson clouds. In particular, restricting the exploration to the parameter space relevant for the expected boson cloud signals significantly reduces the trial factor with a consequent implicit gain in the sensitivity with respect to standard wider parameter space searches.

A second type of interpretation, as shown in Fig. 8, is represented by the maximum distance $D_{\rm max}$ at which we

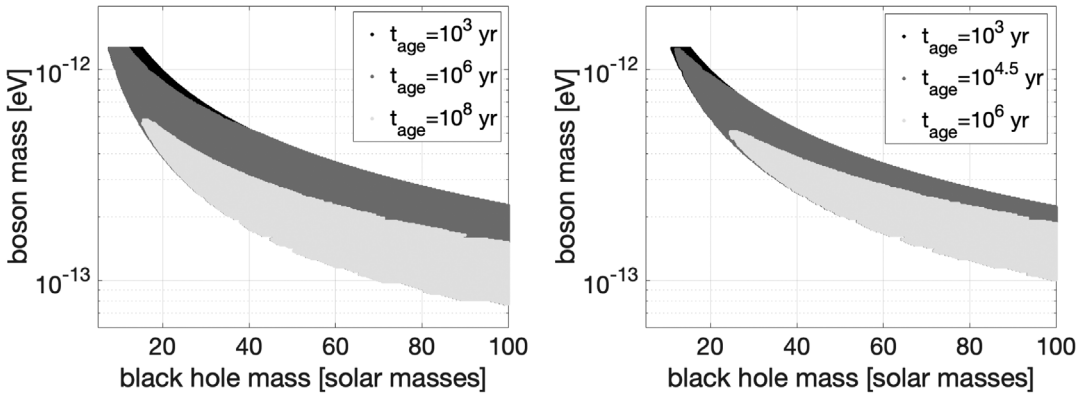

FIG. 6. Exclusion regions in the boson mass (m_b) and black hole mass ($M_{\rm BH}$) plane for an assumed distance of $D = 1$ kpc (left) and $D = 15$ kpc (right), and an initial black hole dimensionless spin $\chi_i = 0.9$. For $D = 1$ kpc, three possible values of the black hole age, $t_{\rm age} = 10^3, 10^6, 10^8$ years, are considered; for $D = 15$ kpc, $t_{\rm age} = 10^3, 10^{4.5}, 10^6$ years are considered.

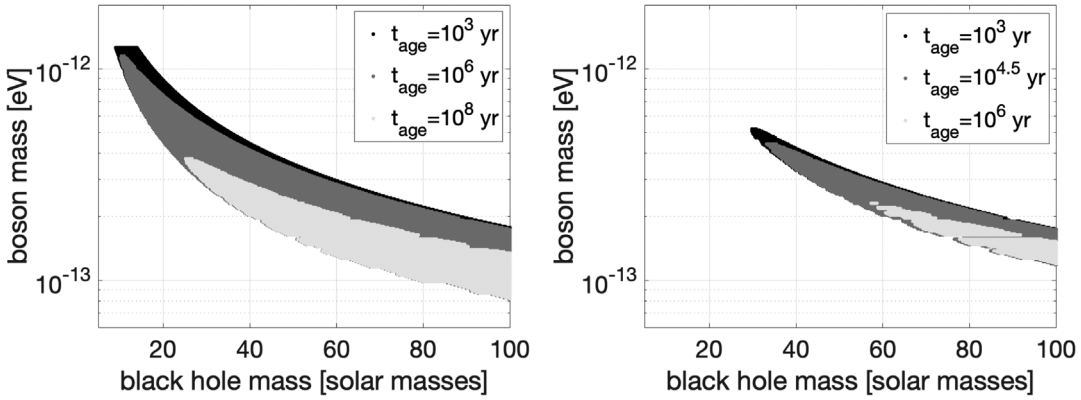

FIG. 7. Same as Fig. 6 but for black hole initial spin $\chi_i = 0.5$. The assumed distance is $D = 1$ kpc (left), and $D = 15$ kpc (right).

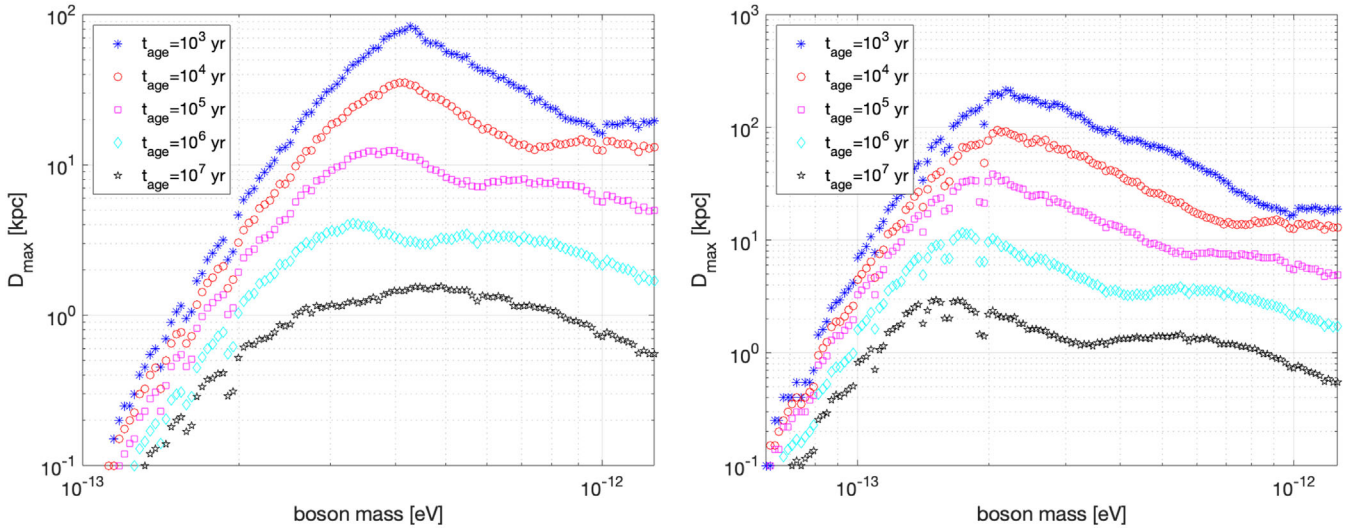

FIG. 8. Maximum distance at which at least 5% of a simulated population of black holes with a boson cloud would produce a gravitational-wave signal with strain amplitude larger than the upper limit in the detectors. The left plot refers to a maximum black hole mass of 50 $M_\odot$, while the right plot to a maximum mass of 100 $M_\odot$. The different colored markers correspond to different system ages, ranging from 10^3 years to 10^7 years, as indicated in the legend. The alignment of points for different ages at the smallest boson masses (and distances) is the result of a discretization effect due to the finite size grid used in distance.

can exclude, as a function of the boson mass, the presence of an emitting system of a given age $t_{\rm age}$, assuming a population of black holes. The black hole population has been simulated using a Kroupa mass distribution, with probability density described by $f(m) \propto m^{-2.3}$ [61], with two different ranges, of $[5, 50]$ $M_\odot$ and $[5, 100]$ $M_\odot$, and a uniform initial spin distribution in the range of [0.2, 0.9]. The criterion to compute $D_{\rm max}$ at a given boson mass is that at least 5% of the simulated signals would produce a strain amplitude larger than the upper limit at the corresponding frequency in the detectors, and thus would have been detected by our search. This choice of 5% should be conservative, given the large black hole population in the galaxy (10^7–10^8) from which we seek a single signal. As before, we correct Eqs. (4) and (9) by a factor of 3 and $\sqrt{3}$, respectively, to obtain more accurate $\tau_{\rm gw}$ and h_0 estimates at $\alpha \gtrsim 0.1$ and thus slightly conservative constraints in the full range. As expected, on average when the maximum black hole mass is smaller, the maximum distance is also smaller, as the signal strain increases with a high power of the black hole mass. Instead of focusing on the specific properties of the emitting system, as for the exclusion regions previously discussed, this constraint on distance depends on the chosen Kroupa mass and uniform spin distributions of the black holes, and thus it reflects the ensemble properties of the assumed black hole population.

Overall, the distance constraints allow us to draw semiquantitative conclusions on the possible presence of emitting boson clouds in our Galaxy. For instance, young systems, with $t_{\rm age}$ smaller than about 10^3 years are disfavored in the whole Galaxy for boson masses above about 2.5×10^{-13} eV for a maximum black hole mass of 50 $M_\odot$ and above about 1.2×10^{-13} eV for a maximum black hole mass of 100 $M_\odot$. As expected, older systems, expected to be more abundant, are more likely to be ruled out only at smaller distances, as they produce on average weaker gravitational-wave signals. As an example, bosons with masses between $\sim 2 \times 10^{-13}$–8×10^{-13} eV ($\sim 10^{-13}$–8×10^{-13} eV) would be excluded within a distance of 1 kpc from Earth for a maximum black hole mass of 50 $M_\odot$ (100 $M_\odot$).

The general shape of the maximum distance curves is a result of the combination of different factors pushing in different directions: higher boson masses tend to produce signals with stronger initial amplitudes, but also faster decay rates as a function of $t_{\rm age}$. Towards the lower m_b end in the plot, $D_{\rm max}$ increases with m_b because the effect of the increasing initial signal amplitudes dominates; towards the higher m_b end, $D_{\rm max}$ tends to decrease again since the faster signal decay rate dominates. At the same time, for higher boson masses, lower black hole masses are required to form a cloud producing signals that last long enough to be detectable. Hence the black hole mass distribution (larger population at lower $M_{\rm BH}$) comes into play as well. In addition, the results are weighted by the frequency-dependent detector sensitivity (reflected in the upper limit curve in Fig. 5), which also affects the final shape of the $D_{\rm max}$ curves.

For both of the constraints presented above, we do not take into account factors that are largely uncertain but could also be relevant to the interpretation, e.g. the black hole spatial distribution or the formation rate. We defer the integration of these factors to future work when they are better constrained.

Concerning the interpretation of our results with respect to the assumed boson self-interaction, the search covers a small range of spin-up values (see Sec. III and, in particular, Fig. 3), mainly corresponding to a regime of small boson self-interaction, i.e. one in which the spin-up is dominated by Eq. (6). For a subset of smaller boson and black hole masses, the spin-up dominated by Eq. (7) in the intermediate regime is also covered in the search. However, as we have clarified in Sec. II, the signal duration is expected to be shorter in this intermediate regime, and the signal amplitude is smaller due to the smaller boson and black hole masses [see Eq. (9)]. Thus the signals in the intermediate regime are less likely to be detected compared to those in the small self-interaction regime.

VI. CONCLUSIONS

This paper describes the first all-sky search tailored to the predicted continuous-wave emission from scalar boson clouds around spinning black holes. We cover a frequency range between 20 and 610 Hz, and a small frequency-dependent spin-up range corresponding to the small self-interaction regime.

We use a multiple frequency-resolution approach, in order to optimize the sensitivity for signals characterized by a slightly wandering frequency, for which a search based on the fixed maximum possible Fourier transform duration would cause a sensitivity loss. No candidate survives the multistep follow-up procedures we have implemented.

Following up outliers in this analysis was significantly more challenging due, in part, to not having a spin-down or spin-up range to consider, typical of standard all-sky continuous-wave analyses, for which instrumental artifacts lead to clusters over extended ranges in source spin-down. Establishing an instrumental source of such clusters is more straightforward in standard analyses than in this analysis. Manual checks by visual inspection of many spectra had to be performed, along with additional methods necessary to reject an outlier due to a transient spectral artifact in H1 (see Sec. C 1). Therefore, this work not only motivates further searches for boson cloud systems but also refined methods to mitigate or conclusively veto persistent or transient spectral disturbances at the level of detector commissioning and characterization.

The resulting upper limits are significantly better than those obtained in previous all-sky searches for continuous

waves, including a recent search in the early O3 data [58], although our search typically covers a much smaller spin-down/up range with respect to those. On the other hand, our upper limits are slightly worse than those obtained in the O2 search carried out with the Falcon pipeline [60], which however was mainly focused on low-ellipticity sources, and thus covered a much smaller spin-down/up range than we do (from a factor of ∼4 at lower frequencies up to a factor of ∼18 at higher frequencies), and moreover did not account for the possibility of signal frequency wandering. The same pipeline was also run from 500–1700 Hz [62] with the same caveats, and although the limits presented in both of these searches are quite stringent, they rely on low-ellipticity sources emitting almost monochromatic gravitational waves. Furthermore, the results in the most recent run of the Falcon pipeline in the 500–600 Hz region using O3a data surpass ours, and could also be interpreted in terms of gravitational-wave emission from boson clouds [63].

Code improvements are possible to make the search more sensitive and computationally more efficient. In this way, future boson cloud searches using the basic methodology adopted in this paper will expand the parameter space, covering a wider frequency band and a larger spin-up range, as well as search for vector boson cloud signals that could have much higher spin-ups than those considered here. This, together with the expected detector improvements in upcoming runs of Advanced LIGO, Advanced Virgo, and KAGRA detectors, will significantly increase the chance of detecting gravitational radiation from these interesting sources, or at least to better constrain the parameter space of these systems.

ACKNOWLEDGMENTS

This material is based upon work supported by NSF's LIGO Laboratory which is a major facility fully funded by the National Science Foundation. The authors also gratefully acknowledge the support of the Science and Technology Facilities Council (STFC) of the United Kingdom, the Max-Planck-Society (MPS), and the State of Niedersachsen/Germany for support of the construction of Advanced LIGO and construction and operation of the GEO600 detector. Additional support for Advanced LIGO was provided by the Australian Research Council. The authors gratefully acknowledge the Italian Istituto Nazionale di Fisica Nucleare (INFN), the French Centre National de la Recherche Scientifique (CNRS) and the Netherlands Organization for Scientific Research (NWO), for the construction and operation of the Virgo detector and the creation and support of the EGO consortium. The authors also gratefully acknowledge research support from these agencies as well as by the Council of Scientific and Industrial Research of India, the Department of Science and Technology, India, the Science and Engineering Research Board (SERB), India, the Ministry of Human Resource Development, India, the Spanish Agencia Estatal de Investigación (AEI), the Spanish Ministerio de Ciencia e Innovación and Ministerio de Universidades, the Conselleria de Fons Europeus, Universitat i Cultura and the Direcció General de Política Universitaria i Recerca del Govern de les Illes Balears, the Conselleria d'Innovació, Universitats, Ciència i Societat Digital de la Generalitat Valenciana, and the CERCA Programme Generalitat de Catalunya, Spain, the National Science Centre of Poland and the European Union—European Regional Development Fund; Foundation for Polish Science (FNP), the Swiss National Science Foundation (SNSF), the Russian Foundation for Basic Research, the Russian Science Foundation, the European Commission, the European Social Funds (ESF), the European Regional Development Funds (ERDF), the Royal Society, the Scottish Funding Council, the Scottish Universities Physics Alliance, the Hungarian Scientific Research Fund (OTKA), the French Lyon Institute of Origins (LIO), the Belgian Fonds de la Recherche Scientifique (FRS-FNRS), Actions de Recherche Concertées (ARC) and Fonds Wetenschappelijk Onderzoek—Vlaanderen (FWO), Belgium, the Paris Île-de-France Region, the National Research, Development and Innovation Office Hungary (NKFIH), the National Research Foundation of Korea, the Natural Science and Engineering Research Council Canada, Canadian Foundation for Innovation (CFI), the Brazilian Ministry of Science, Technology, and Innovations, the International Center for Theoretical Physics South American Institute for Fundamental Research (ICTP-SAIFR), the Research Grants Council of Hong Kong, the National Natural Science Foundation of China (NSFC), the Leverhulme Trust, the Research Corporation, the Ministry of Science and Technology (MOST), Taiwan, the United States Department of Energy, and the Kavli Foundation. The authors gratefully acknowledge the support of the NSF, STFC, INFN, and CNRS for provision of computational resources. This work was supported by MEXT, JSPS Leading-edge Research Infrastructure Program, JSPS Grant-in-Aid for Specially Promoted Research Grant No. 26000005, JSPS Grant-in-Aid for Scientific Research on Innovative Areas 2905: Grants No. JP17H06358, No. JP17H06361, and No. JP17H06364, JSPS Core-to-Core Program A. Advanced Research Networks, JSPS Grant-in-Aid for Scientific Research (S) Grants No. 17H06133 and No. 20H05639, JSPS Grant-in-Aid for Transformative Research Areas (A) 20A203: Grant No. JP20H05854, the joint research program of the Institute for Cosmic Ray Research, University of Tokyo, National Research Foundation (NRF) and Computing Infrastructure Project of KISTI-GSDC in Korea, Academia Sinica (AS), AS Grid Center (ASGC) and the Ministry of Science and Technology (MoST) in Taiwan under grants including AS-CDA-105-M06, Advanced Technology Center (ATC) of NAOJ, Mechanical Engineering Center of KEK.

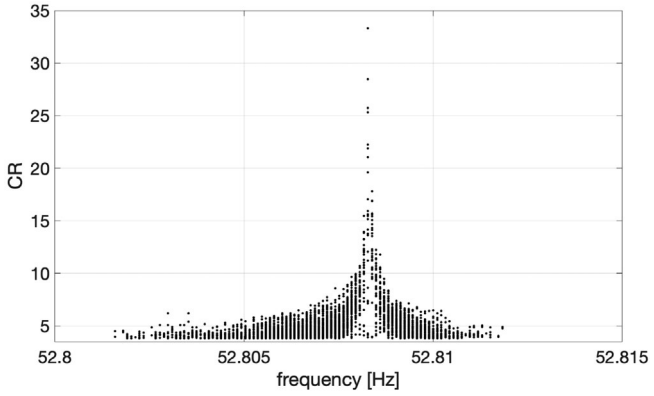

FIG. 9. Critical ratio of the candidates produced by *hardware injection* P5 in H1 data and found in the search with $W = 1$. The distance of the highest CR candidate from the injected signal is about 0.7.

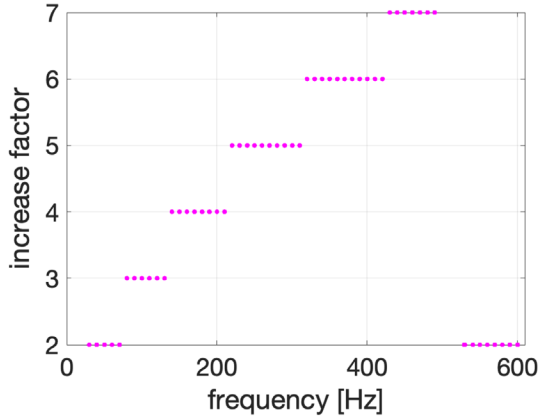

FIG. 10. FFT length increase factor, with respect to the main search FFT length, as a function of frequency for FU1. This factor is reduced at the highest frequencies in order to keep the computer memory used by the analysis jobs under control.

APPENDIX A: HARDWARE INJECTIONS

Both H1 and L1 data contain 14 simulated continuous-wave signals, called *hardware injections*, added via hardware for testing purposes. Only one of them, named P5, is within the searched frequency and $\dot{f}$ range and has an amplitude high enough to be detectable in this search. Indeed we find it with a maximum CR $\simeq 33$ and 36, respectively, in the two detectors (and with an averaged dimensionless distance $d \approx 0.7$). As this injected signal is very strong, it produces tens of thousands of outliers at slightly different points in the parameter space. Thus we remove these outliers caused by the hardware injection P5. Figure 9 shows the outliers found in H1 data caused by this injected signal.

APPENDIX B: FOLLOW-UP METHODOLOGY

Here we provide details about the two methods used for outlier follow-up. The first one, applied to outliers with $W = 1$, is more suitable for monochromatic or nearly monochromatic signals, while the second works well for signals characterized by some amount of frequency fluctuations. In principle, both methods can be applied to all outliers. The sensitivities of the two methods cannot be directly compared since the two methods assume different signal models. To keep the number of outliers at a practical level for both methods, we only use one method for each category. We assume that for outliers with $W = 1$, the impact from any potential random frequency fluctuation is negligible.

1. Follow-up for outliers with $W = 1$

The follow-up for monochromatic or nearly monochromatic signals consists of several steps, applied to each outlier, and is described in detail in [49]. First, given the frequency and sky coordinates of an outlier, the Doppler modulation of a possible gravitational-wave signal is removed from the data by heterodyne.[6] This allows us to build a new set of FFTs, with a longer duration with respect to the original value, as well as the corresponding peakmap. The factor by which the FFTs duration is increased is a function of the frequency and is shown in Fig. 10. It is chosen as a compromise between the need to improve sensitivity and to keep the computational cost of the follow-up under control. Using different lengthening factors at different frequencies aims to produce similar durations for the new set of FFTs, which would correspond to similar follow-up sensitivity, taking into account that the initial FFTs are shorter at higher frequencies (see Fig. 2). In practice, due to computer memory limitations, we have to limit the increase at the highest frequencies between 500 and 600 Hz.

A follow-up volume, defined by ± 3 frequency bins and ± 3 bins for each sky coordinates (these bins, called *coarse* bins, are those of the initial search setup) around the outlier, is considered. For each sky position and frequency in the follow-up volume, by linear extrapolation of the detector velocity vector, we evaluate the residual Doppler modulation (with respect to the center of the grid), which is corrected in the peakmap by properly shifting each peak. This extrapolation procedure is orders of magnitude faster than the exact Doppler correction and is accurate as long as the follow-up volume is sufficiently small (see [49]).

The Frequency-Hough algorithm [38] is then applied to the resulting ensemble of corrected peakmaps (covering ± 1 coarse bin in $\dot{f}$). It maps the detector time-frequency plane of the peakmap to the source frequency-$\dot{f}$ plane. The absolute maximum identified among all frequency-$\dot{f}$ Frequency-Hough histograms provides the refined

[6]This is a standard technique that involves multiplying the data by a phase factor $\exp[-j\phi_d(t)]$, where $\phi_d(t)$ is the time-dependent phase evolution induced by the Doppler effect.

parameters of the original outlier. This procedure is applied to each element of coincident pairs of outliers.

Next, we apply a series of vetoes to each pair of refined outliers, detailed as follows. First, for each detector, a new peakmap is computed using the data coherently corrected with the refined parameters of the outlier and then projected onto the frequency axis. We take the maximum of this projection in a range of ±2 coarse bins around the outlier frequency.[7]

The rest of a 0.2-Hz band around the outlier, which we consider as the "off-source" region, is divided into a frequency-dependent number of intervals of the same width (in practice, this number varies from about 600 at the lowest frequencies, to about 100 at the highest frequencies). We take the maximum of the peakmap projection in each of these intervals and sort all these maxima in a decreasing order. We keep the outlier if it ranks in the 1% top list in both detectors.

Surviving outliers are then subject to three further tests. The first is a test based on the consistency of the outlier CR in the two detectors, similar to that already used in the main search. The second is a test in which an outlier is discarded, if its CR after the follow-up (in both detectors) drops compared to the original CR from the main search. Finally, we discard coincident outliers with $d > 6$ after the follow-up, indicating that they can no longer be considered as coincident. Outliers surviving this first follow-up (FU1) are subject to a second round (FU2) in which the same procedure is used but the FFT duration is further increased. Figure 11 shows the lengthening factor in FU2, as before with respect to the initial duration. The follow-up volume around each outlier consists, as before, of ±3 coarse frequency bins, ±3 bin for each sky coordinate, and ±1 $\dot{f}$ bin around the outlier (note that these are *coarse* bins of the initial main search). If needed, a third follow-up stage along the same line, is applied. The follow-up volume is the same as in previous steps, while the FFT length increase is chosen specifically depending on the outlier parameters. Any outliers surviving these follow-up steps will be eventually analyzed with *ad hoc* methods.

2. Follow-up for outliers with $W > 1$

Outliers found with $W > 1$ are expected to have some level of frequency evolution that leads to power leakage into adjacent frequency bins. We use the Viterbi method, based on a HMM tracking scheme, which has been used in various continuous-wave searches [15,16,64–66]. The Viterbi method can efficiently track secular evolution as well as random fluctuation in the signal frequency,

[7]The ± 2 bins used at this level do not have any particular relation with the ±3 bins used to define the follow-up volume. The latter choice is due to the uncertainty on the parameters of the outlier, while the former is chosen to estimate the outlier significance.

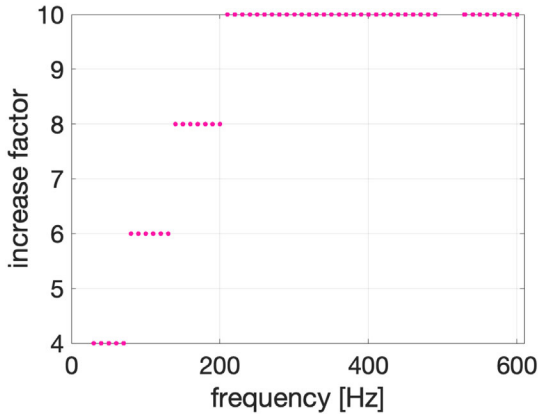

FIG. 11. FFT length increase factor, with respect to the main search length, as a function of frequency for FU2.

and thus is an ideal follow-up tool to verify candidates with $W > 1$.

For each outlier identified with $W > 1$, we first estimate the maximum $\dot{f}$ value assuming that all the signal power is distributed in W frequency bins,

$$\dot{f}_{\max} = \frac{W}{2T_{\mathrm{obs}}T_{\mathrm{FFT}}}, \tag{B1}$$

and select a coherent time T_{coh} such that the $\dot{f}_{\max}$ can be covered in the Viterbi follow-up search. See details about how to select T_{coh} in Sec. IV A of [15]. In this follow-up study, three different values of $T_{\mathrm{coh}} = 1\mathrm{d}$, 2d, and 4d are used, with shorter T_{coh} applied to larger $\dot{f}_{\max}$. For $T_{\mathrm{coh}} = 1\mathrm{d}$, 2d, and 4d, a narrow frequency band of 0.5, 0.125, and 0.03125 Hz, centered at the outlier frequency, is searched, respectively. The best estimated sky position in the main search is used for the follow-up analysis. This follow-up procedure consists of three steps.

First, we search in the combined data from LIGO Hanford and Livingston using the Viterbi method with the T_{coh} and frequency band configurations listed above. The detection score S is defined, such that the log likelihood of the optimal Viterbi path equals the mean log likelihood of all paths ending in different frequency bins plus S standard deviations in each band searched [65]. We discard outliers which are not found in the Viterbi follow-up, either S is below the threshold (corresponding to 1% false alarm probability) or the optimal Viterbi path is completely irrelevant to the original outlier (returned at a nonoverlapping frequency). Second, we eliminate the outliers whose significance is higher when analyzing one detector only than combining the two, while searching the other detector alone yields S below the threshold, i.e. the outlier is dominantly louder in a single detector. Third, we carry out manual inspections for any remaining outliers that survive the first two steps.

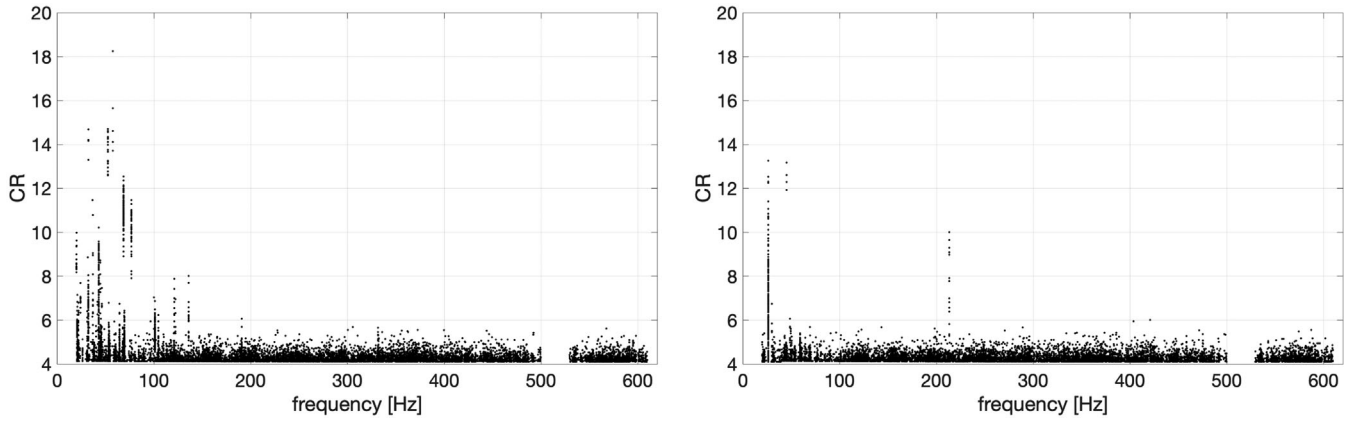

FIG. 12. Critical ratio of the main search H1 (left) and L1 (right) outliers with $W = 1$.

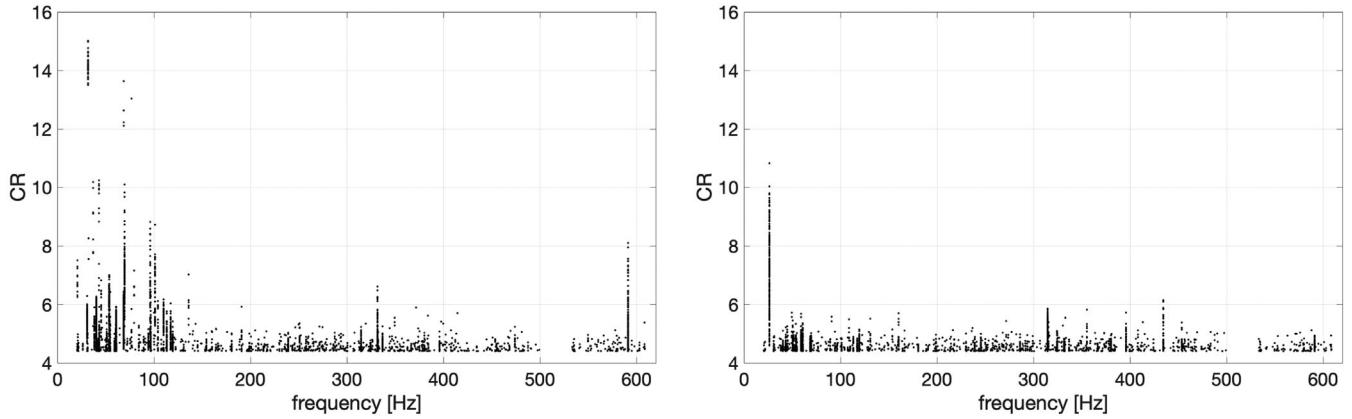

FIG. 13. Critical ratio of the main search H1 (left) and L1 (right) outliers with $W > 1$.

APPENDIX C: CANDIDATES AND FOLLOW-UP RESULTS

The outliers produced by the main search, with average window $W = 1$ and $W > 1$, are shown, respectively, in Figs. 12 and 13 in terms of their CR as a function of the frequency. It is clear that the majority of the strongest outliers is due to H1 data, and is concentrated in the lower frequency range below ∼150 Hz. In the following, we present details of the follow-up results for the outliers.

1. Follow-up results for outliers with $W = 1$

For outliers with $W = 1$, we apply the follow-up procedure described in Appendix B 1.

We start with FU1, which produces outliers with refined parameters, on which various vetoes are applied. The application of the significance veto removes most of the outliers, with only 160 surviving. Among these, 14 are discarded as their CR decreases, and an additional 10 are eliminated because they yield a post-follow-up distance of $d > 6$ (i.e. they are no longer coincident).

The CRs of the 136 outliers passing FU1 are shown, as a function of frequency, in Fig. 14. By visual inspection of the refined time-frequency peakmaps produced in FU1, we are able to conclude that many of the strongest outliers are not compatible with an astrophysical signal. In particular, this happens for 1 outlier at 24.20 Hz, 6 at ∼31.14 Hz, 2 at ∼37.31 Hz, 1 at ∼41.72 Hz, 1 at ∼57.59 Hz, 3 at

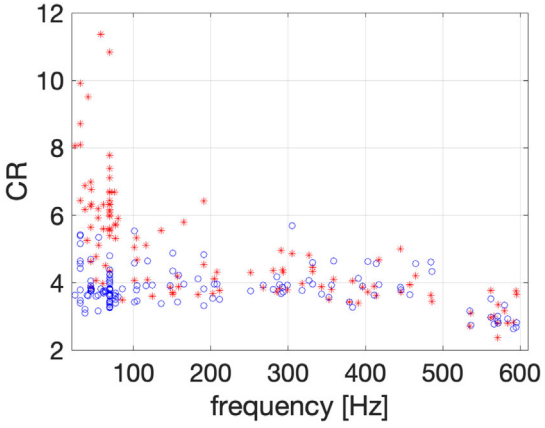

FIG. 14. Critical ratios of outliers passing FU1 follow-up stage as a function of their frequencies (circles: Livingston, stars: Hanford).

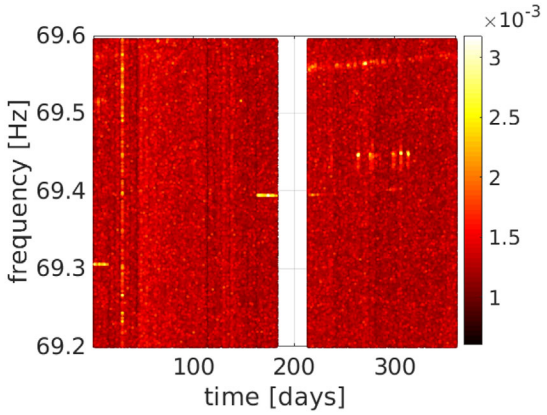

FIG. 15. Time-frequency peakmap of H1 data after FU1 follow-up stage showing a distinct broad disturbance appearing in the second half of the run and responsible for the 22 outliers identified with frequency ∼69.55 Hz. Time is measured in days since the stsrting of the run. The colorbar represents a power spectrum in units of 10^{-40} [1/Hz].

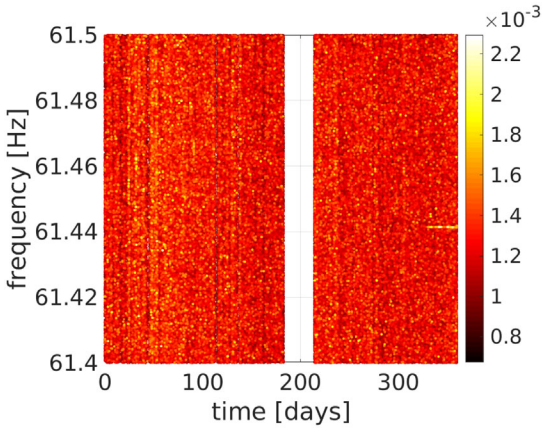

FIG. 16. Time-frequency peakmap of H1 data after FU2 around the outlier with frequency ∼61.44 Hz. Time is measured in days since the starting of the run. A transient disturbance, starting from ∼20 days before the end of the run, is clearly visible. The color bar represents power spectrum in units of 10^{-40} [1/Hz].

∼69.39 Hz, and 22 at ∼69.55 Hz. As an example, we show in Fig. 15 the refined peakmap built from H1 data, indicating a clear transient disturbance in the second half of the run and responsible for the outliers at ∼69.55 Hz.

The remaining 97 outliers are analyzed in FU2, which reduces the number of surviving candidates to three (91 are removed by the significance veto and 3 by the distance veto).

TABLE I. Average parameters of outliers passing FU2.

Frequency (Hz)	λ (deg)	β (deg)	$\dot{f}$ (Hz/s)	CR
61.4416	76.6500	60.5462	-4.6745×10^{-13}	6.1300
104.1381	85.5924	−59.5761	-5.8598×10^{-13}	4.5150
305.1118	23.2246	50.5265	-5.3121×10^{-12}	4.3600

The final three remaining outliers have average parameters (averaged values of the parameters obtained from the two detectors) shown in Table I. The first one, at ∼61.44 Hz, has been discarded by looking at the corresponding refined peakmap, where a transient disturbance in H1 data, starting ∼20 days before the end of the run and at the exact frequency of the candidate, can be identified, see Fig. 16. The other two have been subject to the third follow-up step, with an increase of the FFT duration of, respectively, a factor of 10 and 12 with respect to the initial value used in the main search. Neither of the outliers pass the significance veto and, moreover, the CR reduces for both outliers (in both detectors). Thus we finally discard them as not compatible with astrophysical signals.

2. Follow-up results for outliers with $W > 1$

For the original outliers with $W > 1$, we apply the follow-up procedure described in Sec. B 2. In total, 7816 outliers are identified with $W > 1$ in the main search. After the first step of searching data from both LIGO detectors using the Viterbi method, only a small number of the original outliers (267 out of 7816) are identified above the Viterbi threshold (1% false alarm probability in each sub-band searched). After the second step, in which the Viterbi searches are carried out in data from Hanford and Livingston detectors separately, we eliminate an additional 73 outliers, and the remaining 194 are subject to further manual scrutiny.

Finally, we carry out manual inspections for the remaining 194 outliers, clustered at six different frequencies. We find 178 of them clustered near 26.33 Hz are caused by a pulsar hardware injection in O3, and thus are not of astrophysical origin. Another 15 are associated with various instrumental disturbances. For the last outlier found at ∼190.82 Hz, further investigations in every few days of data find that it results from disturbances around that frequency at the Hanford detector in the last ∼20 days.

[1] J. Preskill, M. B. Wise, and F. Wilczek, Cosmology of the invisible axion, Phys. Lett. B **120**, 127 (1983).

[2] L. F. Abbott and P. Sikivie, A cosmological bound on the invisible axion, Phys. Lett. B **120**, 133 (1983).

[3] M. Dine and W. Fischler, The not so harmless axion, Phys. Lett. B **120**, 137 (1983).

[4] A. Arvanitaki, S. Dimopoulos, S. Dubovsky, N. Kaloper, and J. March-Russell, String axiverse, Phys. Rev. D **81**, 123530 (2010).

[5] A. Arvanitaki and S. Dubovsky, Exploring the string axiverse with precision black hole physics, Phys. Rev. D **83**, 044026 (2011).

[6] A. Arvanitaki, M. Baryakhtar, and X. Huang, Discovering the QCD axion with black holes and gravitational waves, Phys. Rev. D **91**, 084011 (2015).

[7] R. Brito, V. Cardoso, and P. Pani, Superradiance: New frontiers in black hole physics, Lect. Notes Phys. **906**, 1 (2015).

[8] A. Arvanitaki, M. Baryakhtar, S. Dimopoulos, S. Dubovsky, and R. Lasenby, Black hole mergers and the QCD axion at Advanced LIGO, Phys. Rev. D **95**, 043001 (2017).

[9] R. Brito, S. Ghosh, E. Barausse, E. Berti, V. Cardoso, I. Dvorkin, A. Klein, and P. Pani, Gravitational wave searches for ultralight bosons with LIGO and LISA, Phys. Rev. D **96**, 064050 (2017).

[10] M. Baryakhtar, R. Lasenby, and M. Teo, Black hole superradiance signatures of ultralight vectors, Phys. Rev. D **96**, 035019 (2017).

[11] N. Siemonsen and W. E. East, Gravitational wave signatures of ultralight vector bosons from black hole superradiance, Phys. Rev. D **101**, 024019 (2020).

[12] R. Brito, S. Grillo, and P. Pani, Black Hole Superradiant Instability from Ultralight Spin-2 Fields, Phys. Rev. Lett. **124**, 211101 (2020).

[13] M. Baryakhtar, M. Galanis, R. Lasenby, and O. Simon, Black hole superradiance of self-interacting scalar fields, Phys. Rev. D **103**, 095019 (2021).

[14] C. Palomba, S. D'Antonio, P. Astone, S. Frasca, G. Intini, I. La Rosa, P. Leaci, S. Mastrogiovanni, A. L. Miller, F. Muciaccia *et al.*, Direct Constraints on the Ultralight Boson Mass from Searches of Continuous Gravitational Waves, Phys. Rev. Lett. **123**, 171101 (2019).

[15] M. Isi, L. Sun, R. Brito, and A. Melatos, Directed searches for gravitational waves from ultralight bosons, Phys. Rev. D **99**, 084042 (2019).

[16] L. Sun, R. Brito, and M. Isi, Search for ultralight bosons in Cygnus X-1 with Advanced LIGO, Phys. Rev. D **101**, 063020 (2020); **102**, 089902(E) (2020).

[17] S. J. Zhu, M. Baryakhtar, M. A. Papa, D. Tsuna, N. Kawanaka, and H.-B. Eggenstein, Characterizing the continuous gravitational-wave signal from boson clouds around galactic isolated black holes, Phys. Rev. D **102**, 063020 (2020).

[18] L. Pierini *et al.* (to be published).

[19] S. Vitale, R. Lynch, J. Veitch, V. Raymond, and R. Sturani, Measuring the Spin of Black Holes in Binary Systems Using Gravitational Waves, Phys. Rev. Lett. **112**, 251101 (2014).

[20] M. Pürrer, M. Hannam, and F. Ohme, Can we measure individual black-hole spins from gravitational-wave observations?, in *Proceedings of the 14th Marcel Grossmann Meeting on Recent Developments in Theoretical and Experimental General Relativity, Astrophysics, and Relativistic Field Theories* (2017).

[21] K. Belczynski *et al.*, Evolutionary roads leading to low effective spins, high black hole masses, and O1/O2 rates for LIGO/Virgo binary black holes, Astron. Astrophys. **636**, A104 (2020).

[22] D. Gerosa, E. Berti, R. O'Shaughnessy, K. Belczynski, M. Kesden, D. Wysocki, and W. Gladysz, Spin orientations of merging black holes formed from the evolution of stellar binaries, Phys. Rev. D **98**, 084036 (2018).

[23] K. K. Y. Ng, O. A. Hannuksela, S. Vitale, and T. G. F. Li, Searching for ultralight bosons within spin measurements of a population of binary black hole mergers, Phys. Rev. D **103**, 063010 (2021).

[24] K. K. Y. Ng, S. Vitale, O. A. Hannuksela, and T. G. F. Li, Constraints on Ultralight Scalar Bosons within Black Hole Spin Measurements from the LIGO-Virgo GWTC-2, Phys. Rev. Lett. **126**, 151102 (2021).

[25] D. Baumann, H. S. Chia, and R. A. Porto, Probing ultralight bosons with binary black holes, Phys. Rev. D **99**, 044001 (2019).

[26] Q. Yang, L.-W. Ji, B. Hu, Z.-J. Cao, and R.-G. Cai, An axion-like scalar field environment effect on binary black hole merger, Res. Astron. Astrophys. **18**, 065 (2018).

[27] S. Choudhary, N. Sanchis-Gual, A. Gupta, J. C. Degollado, S. Bose, and J. A. Font, Gravitational waves from binary black hole mergers surrounded by scalar field clouds: Numerical simulations and observational implications, Phys. Rev. D **103**, 044032 (2021).

[28] K. K. Y. Ng, M. Isi, C.-J. Haster, and S. Vitale, Multiband gravitational-wave searches for ultralight bosons, Phys. Rev. D **102**, 083020 (2020).

[29] R. Brito, S. Ghosh, E. Barausse, E. Berti, V. Cardoso, I. Dvorkin, A. Klein, and P. Pani, Stochastic and Resolvable Gravitational Waves from Ultralight Bosons, Phys. Rev. Lett. **119**, 131101 (2017).

[30] L. Tsukada, T. Callister, A. Matas, and P. Meyers, First search for a stochastic gravitational-wave background from ultralight bosons, Phys. Rev. D **99**, 103015 (2019).

[31] L. Tsukada, R. Brito, W. E. East, and N. Siemonsen, Modeling and searching for a stochastic gravitational-wave background from ultralight vector bosons, Phys. Rev. D **103**, 083005 (2021).

[32] C. Yuan, R. Brito, and V. Cardoso, Probing ultralight dark matter with future ground-based gravitational-wave detectors, Phys. Rev. D **104**, 044011 (2021).

[33] T. Co. Raymond, A. Pierce, Z. Zhang, Y. Zhao *et al.*, Dark photon dark matter produced by axion oscillations, Phys. Rev. D **99**, 075002 (2019).

[34] A. L. Miller *et al.*, Probing new light gauge bosons with gravitational-wave interferometers using an adapted semi-coherent method, Phys. Rev. D **103**, 103002 (2021).

[35] H.-K. Guo, K. Riles, F.-W. Yang, and Y. Zhao, Searching for dark photon dark matter in LIGO O1 data, Commun. Phys. **2**, 1 (2019).

[36] R. Abbott *et al.*, Constraints on dark photon dark matter using data from LIGO's and Virgo's third observing run, Phys. Rev. D **105**, 063030 (2022).

[37] J. Aasi, B. P. Abbott, R. Abbott, T. Abbott, M. R. Abernathy, K. Ackley, C. Adams, T. Adams, P. Addesso *et al.*, Advanced LIGO, Classical Quantum Gravity **32**, 074001 (2015).
[38] P. Astone, A. Colla, S. D'Antonio, S. Frasca, and C. Palomba, Method for all-sky searches of continuous gravitational wave signals using the Frequency-Hough transform, Phys. Rev. D **90**, 042002 (2014).
[39] K. Riles, Recent searches for continuous gravitational waves, Mod. Phys. Lett. A **32**, 1730035 (2017).
[40] M. Sieniawska and Michał Bejger, Continuous waves from neutron stars: Current status and prospects, Universe **5**, 217 (2019).
[41] R. Tenorio, D. Keitel, and A. M. Sintes, Search methods for continuous gravitational-wave signals from unknown sources in the advanced-detector era, Universe **7**, 474 (2021).
[42] S. D'Antonio, C. Palomba, P. Astone, S. Frasca, G. Intini, I. La Rosa, P. Leaci, S. Mastrogiovanni, A. Miller, F. Muciaccia *et al.*, Semicoherent analysis method to search for continuous gravitational waves emitted by ultralight boson clouds around spinning black holes, Phys. Rev. D **98**, 103017 (2018).
[43] K. S. Thorne, C. W. Misner, and J. A. Wheeler, *Gravitation* (Freeman, San Francisco, 2000).
[44] J. D. Bekenstein, Extraction of energy and charge from a black hole, Phys. Rev. D **7**, 949 (1973).
[45] O. Piccinni, P. Astone, S. D'Antonio, S. Frasca, G. Intini, P. Leaci, S. Mastrogiovanni, A. Miller, C. Palomba, and A. Singhal, A new data analysis framework for the search of continuous gravitational wave signals, Classical Quantum Gravity **36**, 015008 (2019).
[46] O. J. Piccinni, P. Astone, S. D'Antonio, S. Frasca, G. Intini, I. La Rosa, P. Leaci, S. Mastrogiovanni, A. Miller, and C. Palomba, Directed search for continuous gravitational-wave signals from the galactic center in the Advanced LIGO second observing run, Phys. Rev. D **101**, 082004 (2020).
[47] R. Abbott, T. Abbott *et al.*, Searches for continuous gravitational waves from young supernova remnants in the early third observing run of Advanced LIGO and Virgo, Astrophys. J. **921**, 80 (2021).
[48] R. Abbott, T. Abbott, S. Abraham, F. Acernese, K. Ackley, A. Adams, C. Adams, R. Adhikari, V. Adya, C. Affeldt *et al.*, Gravitational-wave constraints on the equatorial ellipticity of millisecond pulsars, Astrophys. J. Lett. **902**, L21 (2020).
[49] B. Abbott *et al.*, All-sky search for continuous gravitational waves from isolated neutron stars using Advanced LIGO O2 data, Phys. Rev. D **100**, 024004 (2019).
[50] B. P. Abbott *et al.*, All-sky search for periodic gravitational waves in the O1 LIGO data, Phys. Rev. D **96**, 062002 (2017).
[51] L. Sun *et al.*, Characterization of systematic error in Advanced LIGO calibration, Classical Quantum Gravity **37**, 225008 (2020).
[52] L. Sun *et al.*, Characterization of systematic error in Advanced LIGO calibration in the second half of O3, 2021.
[53] https://dcc.ligo.org/T2000384/.
[54] https://dcc.ligo.org/T2000512/.
[55] R. Abbott *et al.*, Upper limits on the isotropic gravitational-wave background from Advanced LIGO and Advanced Virgo's third observing run, Phys. Rev. D **104**, 022004 (2021).
[56] M. Di Cesare, All-sky gravitational wave searches for isolated neutron stars: methods and applications to LIGO-Virgo data, Master thesis, University of Rome "Sapienza", 2021, https://web.infn.it/VirgoRoma/images/MartinaDiCesare_MDC_master_thesis.pdf.
[57] R. Abbott *et al.*, All-sky search for continuous gravitational waves from isolated neutron stars using Advanced LIGO and Advanced Virgo O3 data, 2022.
[58] R. Abbott *et al.*, All-sky search for continuous gravitational waves from isolated neutron stars in the early O3 LIGO data, Phys. Rev. D **104**, 082004 (2021).
[59] B. Steltner, M. A. Papa, H. B. Eggenstein, B. Allen, V. Dergachev, R. Prix, B. Machenschalk, S. Walsh, S. J. Zhu, and S. Kwang, Einstein@Home all-sky search for continuous gravitational waves in LIGO O2 public data, Astrophys. J. **909**, 79 (2021).
[60] V. Dergachev and M. A. Papa, The search for continuous gravitational waves from small-ellipticity sources at low frequencies, Phys. Rev. D **104**, 043003 (2021).
[61] O. D. Ebert, J. S. Bullock, and M. Kaplinghat, Counting black holes: The cosmic stellar remnant population and implications for LIGO, Mon. Not. R. Astron. Soc. **473**, 1186 (2018).
[62] V. Dergachev and M. A. Papa, Results from the First All-Sky Search for Continuous Gravitational Waves from Small-Ellipticity Sources, Phys. Rev. Lett. **125**, 171101 (2020).
[63] V. Dergachev and M. A. Papa, A frequency resolved atlas of the sky in continuous gravitational waves, 2022.
[64] S. Suvorova, L. Sun, A. Melatos, W. Moran, and R. J. Evans, Hidden Markov model tracking of continuous gravitational waves from a neutron star with wandering spin, Phys. Rev. D **93**, 123009 (2016).
[65] L. Sun, A. Melatos, S. Suvorova, W. Moran, and R. Evans, Hidden Markov model tracking of continuous gravitational waves from young supernova remnants, Phys. Rev. D **97**, 043013 (2018).
[66] L. Sun and A. Melatos, Application of hidden markov model tracking to the search for long-duration transient gravitational waves from the remnant of the binary neutron star merger GW170817, Phys. Rev. D **99**, 123003 (2019).

R. Abbott,[1] H. Abe,[2] F. Acernese,[3,4] K. Ackley,[5] N. Adhikari,[6] R. X. Adhikari,[1] V. K. Adkins,[7] V. B. Adya,[8] C. Affeldt,[9,10] D. Agarwal,[11] M. Agathos,[12,13] K. Agatsuma,[14] N. Aggarwal,[15] O. D. Aguiar,[16] L. Aiello,[17] A. Ain,[18] P. Ajith,[19]

T. Akutsu,[20,21] S. Albanesi,[22,23] R. A. Alfaidi,[24] A. Allocca,[25,4] P. A. Altin,[8] A. Amato,[26] C. Anand,[5] S. Anand,[1] A. Ananyeva,[1] S. B. Anderson,[1] W. G. Anderson,[6] M. Ando,[27,28] T. Andrade,[29] N. Andres,[30] M. Andrés-Carcasona,[31] T. Andrić,[32] S. V. Angelova,[33] S. Ansoldi,[34,35] J. M. Antelis,[36] S. Antier,[37,38] T. Apostolatos,[39] E. Z. Appavuravther,[40,41] S. Appert,[1] S. K. Apple,[42] K. Arai,[1] A. Araya,[43] M. C. Araya,[1] J. S. Areeda,[44] M. Arène,[45] N. Aritomi,[20] N. Arnaud,[46,47] M. Arogeti,[48] S. M. Aronson,[7] K. G. Arun,[49] H. Asada,[50] Y. Asali,[51] G. Ashton,[52] Y. Aso,[53,54] M. Assiduo,[55,56] S. Assis de Souza Melo,[47] S. M. Aston,[57] P. Astone,[58] F. Aubin,[56] K. AultONeal,[36] C. Austin,[7] S. Babak,[45] F. Badaracco,[59] M. K. M. Bader,[60] C. Badger,[61] S. Bae,[62] Y. Bae,[63] A. M. Baer,[64] S. Bagnasco,[23] Y. Bai,[1] J. Baird,[45] R. Bajpai,[65] T. Baka,[66] M. Ball,[67] G. Ballardin,[47] S. W. Ballmer,[68] A. Balsamo,[64] G. Baltus,[69] S. Banagiri,[15] B. Banerjee,[32] D. Bankar,[11] J. C. Barayoga,[1] C. Barbieri,[70,71,72] B. C. Barish,[1] D. Barker,[73] P. Barneo,[29] F. Barone,[74,4] B. Barr,[24] L. Barsotti,[75] M. Barsuglia,[45] D. Barta,[76] J. Bartlett,[73] M. A. Barton,[24] I. Bartos,[77] S. Basak,[19] R. Bassiri,[78] A. Basti,[79,18] M. Bawaj,[40,80] J. C. Bayley,[24] M. Bazzan,[81,82] B. R. Becher,[83] B. Bécsy,[84] V. M. Bedakihale,[85] F. Beirnaert,[86] M. Bejger,[87] I. Belahcene,[46] V. Benedetto,[88] D. Beniwal,[89] M. G. Benjamin,[90] T. F. Bennett,[91] J. D. Bentley,[14] M. BenYaala,[33] S. Bera,[11] M. Berbel,[92] F. Bergamin,[9,10] B. K. Berger,[78] S. Bernuzzi,[13] D. Bersanetti,[93] A. Bertolini,[60] J. Betzwieser,[57] D. Beveridge,[94] R. Bhandare,[95] A. V. Bhandari,[11] U. Bhardwaj,[38,60] R. Bhatt,[1] D. Bhattacharjee,[96] S. Bhaumik,[77] A. Bianchi,[60,97] I. A. Bilenko,[98] G. Billingsley,[1] S. Bini,[99,100] R. Birney,[101] O. Birnholtz,[102] S. Biscans,[1,75] M. Bischi,[55,56] S. Biscoveanu,[75] A. Bisht,[9,10] B. Biswas,[11] M. Bitossi,[47,18] M.-A. Bizouard,[37] J. K. Blackburn,[1] C. D. Blair,[94] D. G. Blair,[94] R. M. Blair,[73] F. Bobba,[103,104] N. Bode,[9,10] M. Boër,[37] G. Bogaert,[37] M. Boldrini,[105,58] G. N. Bolingbroke,[89] L. D. Bonavena,[81] F. Bondu,[106] E. Bonilla,[78] R. Bonnand,[30] P. Booker,[9,10] B. A. Boom,[60] R. Bork,[1] V. Boschi,[18] N. Bose,[107] S. Bose,[11] V. Bossilkov,[94] V. Boudart,[69] Y. Bouffanais,[81,82] A. Bozzi,[47] C. Bradaschia,[18] P. R. Brady,[6] A. Bramley,[57] A. Branch,[57] M. Branchesi,[32,108] J. E. Brau,[67] M. Breschi,[13] T. Briant,[109] J. H. Briggs,[24] A. Brillet,[37] M. Brinkmann,[9,10] P. Brockill,[6] A. F. Brooks,[1] J. Brooks,[47] D. D. Brown,[89] S. Brunett,[1] G. Bruno,[59] R. Bruntz,[64] J. Bryant,[14] F. Bucci,[56] T. Bulik,[110] H. J. Bulten,[60] A. Buonanno,[111,112] K. Burtnyk,[73] R. Buscicchio,[14] D. Buskulic,[30] C. Buy,[113] R. L. Byer,[78] G. S. Cabourn Davies,[52] G. Cabras,[34,35] R. Cabrita,[59] L. Cadonati,[48] M. Caesar,[114] G. Cagnoli,[26] C. Cahillane,[73] J. Calderón Bustillo,[115] J. D. Callaghan,[24] T. A. Callister,[116,117] E. Calloni,[25,4] J. Cameron,[94] J. B. Camp,[118] M. Canepa,[119,93] S. Canevarolo,[66] M. Cannavacciuolo,[103] K. C. Cannon,[28] H. Cao,[89] Z. Cao,[120] E. Capocasa,[45,20] E. Capote,[68] G. Carapella,[103,104] F. Carbognani,[47] M. Carlassara,[9,10] J. B. Carlin,[121] M. F. Carney,[15] M. Carpinelli,[122,123,47] G. Carrillo,[67] G. Carullo,[79,18] T. L. Carver,[17] J. Casanueva Diaz,[47] C. Casentini,[124,125] G. Castaldi,[126] S. Caudill,[60,66] M. Cavaglià,[96] F. Cavalier,[46] R. Cavalieri,[47] G. Cella,[18] P. Cerdá-Durán,[127] E. Cesarini,[125] W. Chaibi,[37] S. Chalathadka Subrahmanya,[128] E. Champion,[129] C.-H. Chan,[130] C. Chan,[28] C. L. Chan,[131] K. Chan,[131] M. Chan,[132] K. Chandra,[107] I. P. Chang,[130] P. Chanial,[47] S. Chao,[130] C. Chapman-Bird,[24] P. Charlton,[133] E. A. Chase,[15] E. Chassande-Mottin,[45] C. Chatterjee,[94] Debarati Chatterjee,[11] Deep Chatterjee,[6] M. Chaturvedi,[95] S. Chaty,[45] C. Chen,[134,135] D. Chen,[53] H. Y. Chen,[75] J. Chen,[130] K. Chen,[136] X. Chen,[94] Y.-B. Chen,[137] Y.-R. Chen,[138] Z. Chen,[17] H. Cheng,[77] C. K. Cheong,[131] H. Y. Cheung,[131] H. Y. Chia,[77] F. Chiadini,[139,104] C-Y. Chiang,[140] G. Chiarini,[82] R. Chierici,[141] A. Chincarini,[93] M. L. Chiofalo,[79,18] A. Chiummo,[47] R. K. Choudhary,[94] S. Choudhary,[11] N. Christensen,[37] Q. Chu,[94] Y-K. Chu,[140] S. S. Y. Chua,[8] K. W. Chung,[61] G. Ciani,[81,82] P. Ciecielag,[87] M. Cieślar,[87] M. Cifaldi,[124,125] A. A. Ciobanu,[89] R. Ciolfi,[142,82] F. Cipriano,[37] F. Clara,[73] J. A. Clark,[1,48] P. Clearwater,[143] S. Clesse,[144] F. Cleva,[37] E. Coccia,[32,108] E. Codazzo,[32] P.-F. Cohadon,[109] D. E. Cohen,[46] M. Colleoni,[145] C. G. Collette,[146] A. Colombo,[70,71] M. Colpi,[70,71] C. M. Compton,[73] M. Constancio Jr.,[16] L. Conti,[82] S. J. Cooper,[14] P. Corban,[57] T. R. Corbitt,[7] I. Cordero-Carrión,[147] S. Corezzi,[80,40] K. R. Corley,[51] N. J. Cornish,[84] D. Corre,[46] A. Corsi,[148] S. Cortese,[47] C. A. Costa,[16] R. Cotesta,[112] R. Cottingham,[57] M. W. Coughlin,[149] J.-P. Coulon,[37] S. T. Countryman,[51] B. Cousins,[150] P. Couvares,[1] D. M. Coward,[94] M. J. Cowart,[57] D. C. Coyne,[1] R. Coyne,[151] J. D. E. Creighton,[6] T. D. Creighton,[90] A. W. Criswell,[149] M. Croquette,[109] S. G. Crowder,[152] J. R. Cudell,[69] T. J. Cullen,[7] A. Cumming,[24] R. Cummings,[24] L. Cunningham,[24] E. Cuoco,[47,153,18] M. Curyło,[110] P. Dabadie,[26] T. Dal Canton,[46] S. Dall'Osso,[32] G. Dálya,[86,154] A. Dana,[78] B. D'Angelo,[119,93] S. Danilishin,[155,60] S. D'Antonio,[125] K. Danzmann,[9,10] C. Darsow-Fromm,[128] A. Dasgupta,[85] L. E. H. Datrier,[24] Sayak Datta,[11] Sayantani Datta,[49] V. Dattilo,[47] I. Dave,[95] M. Davier,[46] D. Davis,[1] M. C. Davis,[114] E. J. Daw,[156] R. Dean,[114] D. DeBra,[78] M. Deenadayalan,[11] J. Degallaix,[157] M. De Laurentis,[25,4] S. Deléglise,[109] V. Del Favero,[129] F. De Lillo,[59] N. De Lillo,[24] D. Dell'Aquila,[122] W. Del Pozzo,[79,18] L. M. DeMarchi,[15] F. De Matteis,[124,125] V. D'Emilio,[17] N. Demos,[75] T. Dent,[115] A. Depasse,[59] R. De Pietri,[158,159] R. De Rosa,[25,4] C. De Rossi,[47] R. DeSalvo,[126,160] R. De Simone,[139] S. Dhurandhar,[11] M. C. Díaz,[90] N. A. Didio,[68] T. Dietrich,[112] L. Di Fiore,[4] C. Di Fronzo,[14] C. Di Giorgio,[103,104] F. Di Giovanni,[127] M. Di Giovanni,[32] T. Di Girolamo,[25,4] A. Di Lieto,[79,18] A. Di Michele,[80] B. Ding,[146] S. Di Pace,[105,58]

I. Di Palma,[105,58] F. Di Renzo,[79,18] A. K. Divakarla,[77] A. Dmitriev,[14] Z. Doctor,[15] L. Donahue,[161] L. D'Onofrio,[25,4] F. Donovan,[75] K. L. Dooley,[17] S. Doravari,[11] M. Drago,[105,58] J. C. Driggers,[73] Y. Drori,[1] J.-G. Ducoin,[46] P. Dupej,[24] U. Dupletsa,[32] O. Durante,[103,104] D. D'Urso,[122,123] P.-A. Duverne,[46] S. E. Dwyer,[73] C. Eassa,[73] P. J. Easter,[5] M. Ebersold,[162] T. Eckhardt,[128] G. Eddolls,[24] B. Edelman,[67] T. B. Edo,[1] O. Edy,[52] A. Effler,[57] S. Eguchi,[132] J. Eichholz,[8] S. S. Eikenberry,[77] M. Eisenmann,[30,20] R. A. Eisenstein,[75] A. Ejlli,[17] E. Engelby,[44] Y. Enomoto,[27] L. Errico,[25,4] R. C. Essick,[163] H. Estellés,[145] D. Estevez,[164] Z. Etienne,[165] T. Etzel,[1] M. Evans,[75] T. M. Evans,[57] T. Evstafyeva,[12] B. E. Ewing,[150] F. Fabrizi,[55,56] F. Faedi,[56] V. Fafone,[124,125,32] H. Fair,[68] S. Fairhurst,[17] P. C. Fan,[161] A. M. Farah,[166] S. Farinon,[93] B. Farr,[67] W. M. Farr,[116,117] E. J. Fauchon-Jones,[17] G. Favaro,[81] M. Favata,[167] M. Fays,[69] M. Fazio,[168] J. Feicht,[1] M. M. Fejer,[78] E. Fenyvesi,[76,169] D. L. Ferguson,[170] A. Fernandez-Galiana,[75] I. Ferrante,[79,18] T. A. Ferreira,[16] F. Fidecaro,[79,18] P. Figura,[110] A. Fiori,[18,79] I. Fiori,[47] M. Fishbach,[15] R. P. Fisher,[64] R. Fittipaldi,[171,104] V. Fiumara,[172,104] R. Flaminio,[30,20] E. Floden,[149] H. K. Fong,[28] J. A. Font,[127,173] B. Fornal,[160] P. W. F. Forsyth,[8] A. Franke,[128] S. Frasca,[105,58] F. Frasconi,[18] J. P. Freed,[36] Z. Frei,[154] A. Freise,[60,97] O. Freitas,[174] R. Frey,[67] P. Fritschel,[75] V. V. Frolov,[57] G. G. Fronzé,[23] Y. Fujii,[175] Y. Fujikawa,[176] Y. Fujimoto,[177] P. Fulda,[77] M. Fyffe,[57] H. A. Gabbard,[24] B. U. Gadre,[112] J. R. Gair,[112] J. Gais,[131] S. Galaudage,[5] R. Gamba,[13] D. Ganapathy,[75] A. Ganguly,[11] D. Gao,[178] S. G. Gaonkar,[11] B. Garaventa,[93,119] C. García Núñez,[101] C. García-Quirós,[145] F. Garufi,[25,4] B. Gateley,[73] V. Gayathri,[77] G.-G. Ge,[178] G. Gemme,[93] A. Gennai,[18] J. George,[95] O. Gerberding,[128] L. Gergely,[179] P. Gewecke,[128] S. Ghonge,[48] Abhirup Ghosh,[112] Archisman Ghosh,[86] Shaon Ghosh,[167] Shrobana Ghosh,[17] Tathagata Ghosh,[11] B. Giacomazzo,[70,71,72] L. Giacoppo,[105,58] J. A. Giaime,[7,57] K. D. Giardina,[57] D. R. Gibson,[101] C. Gier,[33] M. Giesler,[180] P. Giri,[18,79] F. Gissi,[88] S. Gkaitatzis,[18,79] J. Glanzer,[7] A. E. Gleckl,[44] P. Godwin,[150] E. Goetz,[181] R. Goetz,[77] N. Gohlke,[9,10] J. Golomb,[1] B. Goncharov,[32] G. González,[7] M. Gosselin,[47] R. Gouaty,[30] D. W. Gould,[8] S. Goyal,[19] B. Grace,[8] A. Grado,[182,4] V. Graham,[24] M. Granata,[157] V. Granata,[103] A. Grant,[24] S. Gras,[75] P. Grassia,[1] C. Gray,[73] R. Gray,[24] G. Greco,[40] A. C. Green,[77] R. Green,[17] A. M. Gretarsson,[36] E. M. Gretarsson,[36] D. Griffith,[1] W. L. Griffiths,[17] H. L. Griggs,[48] G. Grignani,[80,40] A. Grimaldi,[99,100] E. Grimes,[36] S. J. Grimm,[32,108] H. Grote,[17] S. Grunewald,[112] P. Gruning,[46] A. S. Gruson,[44] D. Guerra,[127] G. M. Guidi,[55,56] A. R. Guimaraes,[7] G. Guixé,[29] H. K. Gulati,[85] A. M. Gunny,[75] H.-K. Guo,[160] Y. Guo,[60] Anchal Gupta,[1] Anuradha Gupta,[183] I. M. Gupta,[150] P. Gupta,[60,66] S. K. Gupta,[107] R. Gustafson,[184] F. Guzman,[185] S. Ha,[186] I. P. W. Hadiputrawan,[136] L. Haegel,[45] S. Haino,[140] O. Halim,[35] E. D. Hall,[75] E. Z. Hamilton,[162] G. Hammond,[24] W.-B. Han,[187] M. Haney,[162] J. Hanks,[73] C. Hanna,[150] M. D. Hannam,[17] O. Hannuksela,[66,60] H. Hansen,[73] T. J. Hansen,[36] J. Hanson,[57] T. Harder,[37] K. Haris,[60,66] J. Harms,[32,108] G. M. Harry,[42] I. W. Harry,[52] D. Hartwig,[128] K. Hasegawa,[188] B. Haskell,[87] C.-J. Haster,[75] J. S. Hathaway,[129] K. Hattori,[189] K. Haughian,[24] H. Hayakawa,[190] K. Hayama,[132] F. J. Hayes,[24] J. Healy,[129] A. Heidmann,[109] A. Heidt,[9,10] M. C. Heintze,[57] J. Heinze,[9,10] J. Heinzel,[75] H. Heitmann,[37] F. Hellman,[191] P. Hello,[46] A. F. Helmling-Cornell,[67] G. Hemming,[47] M. Hendry,[24] I. S. Heng,[24] E. Hennes,[60] J. Hennig,[192] M. H. Hennig,[192] C. Henshaw,[48] A. G. Hernandez,[91] F. Hernandez Vivanco,[5] M. Heurs,[9,10] A. L. Hewitt,[193] S. Higginbotham,[17] S. Hild,[155,60] P. Hill,[33] Y. Himemoto,[194] A. S. Hines,[185] N. Hirata,[20] C. Hirose,[176] T-C. Ho,[136] S. Hochheim,[9,10] D. Hofman,[157] J. N. Hohmann,[128] D. G. Holcomb,[114] N. A. Holland,[8] I. J. Hollows,[156] Z. J. Holmes,[89] K. Holt,[57] D. E. Holz,[166] Q. Hong,[130] J. Hough,[24] S. Hourihane,[1] E. J. Howell,[94] C. G. Hoy,[17] D. Hoyland,[14] A. Hreibi,[9,10] B-H. Hsieh,[188] H-F. Hsieh,[195] C. Hsiung,[134] Y. Hsu,[130] H-Y. Huang,[140] P. Huang,[178] Y-C. Huang,[138] Y.-J. Huang,[140] Yiting Huang,[152] Yiwen Huang,[75] M. T. Hübner,[5] A. D. Huddart,[196] B. Hughey,[36] D. C. Y. Hui,[197] V. Hui,[30] S. Husa,[145] S. H. Huttner,[24] R. Huxford,[150] T. Huynh-Dinh,[57] S. Ide,[198] B. Idzkowski,[110] A. Iess,[124,125] K. Inayoshi,[199] Y. Inoue,[136] P. Iosif,[200] M. Isi,[75] K. Isleif,[128] K. Ito,[201] Y. Itoh,[177,202] B. R. Iyer,[19] V. JaberianHamedan,[94] T. Jacqmin,[109] P.-E. Jacquet,[109] S. J. Jadhav,[203] S. P. Jadhav,[11] T. Jain,[12] A. L. James,[17] A. Z. Jan,[170] K. Jani,[204] J. Janquart,[66,60] K. Janssens,[205,37] N. N. Janthalur,[203] P. Jaranowski,[206] D. Jariwala,[77] R. Jaume,[145] A. C. Jenkins,[61] K. Jenner,[89] C. Jeon,[207] W. Jia,[75] J. Jiang,[77] H.-B. Jin,[208,209] G. R. Johns,[64] R. Johnston,[24] A. W. Jones,[94] D. I. Jones,[210] P. Jones,[14] R. Jones,[24] P. Joshi,[150] L. Ju,[94] A. Jue,[160] P. Jung,[63] K. Jung,[186] J. Junker,[9,10] V. Juste,[164] K. Kaihotsu,[201] T. Kajita,[211] M. Kakizaki,[189] C. V. Kalaghatgi,[17,66,60,212] V. Kalogera,[15] B. Kamai,[1] M. Kamiizumi,[190] N. Kanda,[177,202] S. Kandhasamy,[11] G. Kang,[213] J. B. Kanner,[1] Y. Kao,[130] S. J. Kapadia,[19] D. P. Kapasi,[8] C. Karathanasis,[31] S. Karki,[96] R. Kashyap,[150] M. Kasprzack,[1] W. Kastaun,[9,10] T. Kato,[188] S. Katsanevas,[47] E. Katsavounidis,[75] W. Katzman,[57] T. Kaur,[94] K. Kawabe,[73] K. Kawaguchi,[188] F. Kéfélian,[37] D. Keitel,[145] J. S. Key,[214] S. Khadka,[78] F. Y. Khalili,[98] S. Khan,[17] T. Khanam,[148] E. A. Khazanov,[215] N. Khetan,[32,108] M. Khursheed,[95] N. Kijbunchoo,[8] A. Kim,[15] C. Kim,[207] J. C. Kim,[216] J. Kim,[217] K. Kim,[207] W. S. Kim,[63] Y.-M. Kim,[186] C. Kimball,[15] N. Kimura,[190] M. Kinley-Hanlon,[24] R. Kirchhoff,[9,10] J. S. Kissel,[73] S. Klimenko,[77] T. Klinger,[12] A. M. Knee,[181] T. D. Knowles,[165] N. Knust,[9,10] E. Knyazev,[75] Y. Kobayashi,[177] P. Koch,[9,10] G. Koekoek,[60,155] K. Kohri,[218] K. Kokeyama,[219] S. Koley,[32]

P. Kolitsidou,[17] M. Kolstein,[31] K. Komori,[75] V. Kondrashov,[1] A. K. H. Kong,[195] A. Kontos,[83] N. Koper,[9,10] M. Korobko,[128] M. Kovalam,[94] N. Koyama,[176] D. B. Kozak,[1] C. Kozakai,[53] V. Kringel,[9,10] N. V. Krishnendu,[9,10] A. Królak,[220,221] G. Kuehn,[9,10] F. Kuei,[130] P. Kuijer,[60] S. Kulkarni,[183] A. Kumar,[203] Prayush Kumar,[19] Rahul Kumar,[73] Rakesh Kumar,[85] J. Kume,[28] K. Kuns,[75] Y. Kuromiya,[201] S. Kuroyanagi,[222,223] K. Kwak,[186] G. Lacaille,[24] P. Lagabbe,[30] D. Laghi,[113] E. Lalande,[224] M. Lalleman,[205] T. L. Lam,[131] A. Lamberts,[37,225] M. Landry,[73] B. B. Lane,[75] R. N. Lang,[75] J. Lange,[170] B. Lantz,[78] I. La Rosa,[30] A. Lartaux-Vollard,[46] P. D. Lasky,[5] M. Laxen,[57] A. Lazzarini,[1] C. Lazzaro,[81,82] P. Leaci,[105,58] S. Leavey,[9,10] S. LeBohec,[160] Y. K. Lecoeuche,[181] E. Lee,[188] H. M. Lee,[226] H. W. Lee,[216] K. Lee,[227] R. Lee,[138] I. N. Legred,[1] J. Lehmann,[9,10] A. Lemaître,[228] M. Lenti,[56,229] M. Leonardi,[20] E. Leonova,[38] N. Leroy,[46] N. Letendre,[30] C. Levesque,[224] Y. Levin,[5] J. N. Leviton,[184] K. Leyde,[45] A. K. Y. Li,[1] B. Li,[130] J. Li,[15] K. L. Li,[230] P. Li,[231] T. G. F. Li,[131] X. Li,[137] C-Y. Lin,[232] E. T. Lin,[195] F-K. Lin,[140] F-L. Lin,[233] H. L. Lin,[136] L. C.-C. Lin,[230] F. Linde,[212,60] S. D. Linker,[126,91] J. N. Linley,[24] T. B. Littenberg,[234] G. C. Liu,[134] J. Liu,[94] K. Liu,[130] X. Liu,[6] F. Llamas,[90] R. K. L. Lo,[1] T. Lo,[130] L. T. London,[38,75] A. Longo,[235] D. Lopez,[162] M. Lopez Portilla,[66] M. Lorenzini,[124,125] V. Loriette,[236] M. Lormand,[57] G. Losurdo,[18] T. P. Lott,[48] J. D. Lough,[9,10] C. O. Lousto,[129] G. Lovelace,[44] J. F. Lucaccioni,[237] H. Lück,[9,10] D. Lumaca,[124,125] A. P. Lundgren,[52] L.-W. Luo,[140] J. E. Lynam,[64] M. Ma'arif,[136] R. Macas,[52] J. B. Machtinger,[15] M. MacInnis,[75] D. M. Macleod,[17] I. A. O. MacMillan,[1] A. Macquet,[37] I. Magaña Hernandez,[6] C. Magazzù,[18] R. M. Magee,[1] R. Maggiore,[14] M. Magnozzi,[93,119] S. Mahesh,[165] E. Majorana,[105,58] I. Maksimovic,[236] S. Maliakal,[1] A. Malik,[95] N. Man,[37] V. Mandic,[149] V. Mangano,[105,58] G. L. Mansell,[73,75] M. Manske,[6] M. Mantovani,[47] M. Mapelli,[81,82] F. Marchesoni,[41,40,238] D. Marín Pina,[29] F. Marion,[30] Z. Mark,[137] S. Márka,[51] Z. Márka,[51] C. Markakis,[12] A. S. Markosyan,[78] A. Markowitz,[1] E. Maros,[1] A. Marquina,[147] S. Marsat,[45] F. Martelli,[55,56] I. W. Martin,[24] R. M. Martin,[167] M. Martinez,[31] V. A. Martinez,[77] V. Martinez,[26] K. Martinovic,[61] D. V. Martynov,[14] E. J. Marx,[75] H. Masalehdan,[128] K. Mason,[75] E. Massera,[156] A. Masserot,[30] M. Masso-Reid,[24] S. Mastrogiovanni,[45] A. Matas,[112] M. Mateu-Lucena,[145] F. Matichard,[1,75] M. Matiushechkina,[9,10] N. Mavalvala,[75] J. J. McCann,[94] R. McCarthy,[73] D. E. McClelland,[8] P. K. McClincy,[150] S. McCormick,[57] L. McCuller,[75] G. I. McGhee,[24] S. C. McGuire,[57] C. McIsaac,[52] J. McIver,[181] T. McRae,[8] S. T. McWilliams,[165] D. Meacher,[6] M. Mehmet,[9,10] A. K. Mehta,[112] Q. Meijer,[66] A. Melatos,[121] D. A. Melchor,[44] G. Mendell,[73] A. Menendez-Vazquez,[31] C. S. Menoni,[168] R. A. Mercer,[6] L. Mereni,[157] K. Merfeld,[67] E. L. Merilh,[57] J. D. Merritt,[67] M. Merzougui,[37] S. Meshkov,[1,†] C. Messenger,[24] C. Messick,[75] P. M. Meyers,[121] F. Meylahn,[9,10] A. Mhaske,[11] A. Miani,[99,100] H. Miao,[14] I. Michaloliakos,[77] C. Michel,[157] Y. Michimura,[27] H. Middleton,[121] D. P. Mihaylov,[112] L. Milano,[25,†] A. L. Miller,[59] A. Miller,[91] B. Miller,[38,60] M. Millhouse,[121] J. C. Mills,[17] E. Milotti,[239,35] Y. Minenkov,[125] N. Mio,[240] Ll. M. Mir,[31] M. Miravet-Tenés,[127] A. Mishkin,[77] C. Mishra,[241] T. Mishra,[77] T. Mistry,[156] S. Mitra,[11] V. P. Mitrofanov,[98] G. Mitselmakher,[77] R. Mittleman,[75] O. Miyakawa,[190] K. Miyo,[190] S. Miyoki,[190] Geoffrey Mo,[75] L. M. Modafferi,[145] E. Moguel,[237] K. Mogushi,[96] S. R. P. Mohapatra,[75] S. R. Mohite,[6] I. Molina,[44] M. Molina-Ruiz,[191] M. Mondin,[91] M. Montani,[55,56] C. J. Moore,[14] J. Moragues,[145] D. Moraru,[73] F. Morawski,[87] A. More,[11] C. Moreno,[36] G. Moreno,[73] Y. Mori,[201] S. Morisaki,[6] N. Morisue,[177] Y. Moriwaki,[189] B. Mours,[164] C. M. Mow-Lowry,[60,97] S. Mozzon,[52] F. Muciaccia,[105,58] Arunava Mukherjee,[242] D. Mukherjee,[150] Soma Mukherjee,[90] Subroto Mukherjee,[85] Suvodip Mukherjee,[163,38] N. Mukund,[9,10] A. Mullavey,[57] J. Munch,[89] E. A. Muñiz,[68] P. G. Murray,[24] R. Musenich,[93,119] S. Muusse,[89] S. L. Nadji,[9,10] K. Nagano,[243] A. Nagar,[23,244] K. Nakamura,[20] H. Nakano,[245] M. Nakano,[188] Y. Nakayama,[201] V. Napolano,[47] I. Nardecchia,[124,125] T. Narikawa,[188] H. Narola,[66] L. Naticchioni,[58] B. Nayak,[91] R. K. Nayak,[246] B. F. Neil,[94] J. Neilson,[88,104] A. Nelson,[185] T. J. N. Nelson,[57] M. Nery,[9,10] P. Neubauer,[237] A. Neunzert,[214] K. Y. Ng,[75] S. W. S. Ng,[89] C. Nguyen,[45] P. Nguyen,[67] T. Nguyen,[75] L. Nguyen Quynh,[247] J. Ni,[149] W.-T. Ni,[208,178,138] S. A. Nichols,[7] T. Nishimoto,[188] A. Nishizawa,[28] S. Nissanke,[38,60] E. Nitoglia,[141] F. Nocera,[47] M. Norman,[17] C. North,[17] S. Nozaki,[189] G. Nurbek,[90] L. K. Nuttall,[52] Y. Obayashi,[188] J. Oberling,[73] B. D. O'Brien,[77] J. O'Dell,[196] E. Oelker,[24] W. Ogaki,[188] G. Oganesyan,[32,108] J. J. Oh,[63] K. Oh,[197] S. H. Oh,[63] M. Ohashi,[190] T. Ohashi,[177] M. Ohkawa,[176] F. Ohme,[9,10] H. Ohta,[28] M. A. Okada,[16] Y. Okutani,[198] C. Olivetto,[47] K. Oohara,[188,248] R. Oram,[57] B. O'Reilly,[57] R. G. Ormiston,[149] N. D. Ormsby,[64] R. O'Shaughnessy,[129] E. O'Shea,[180] S. Oshino,[190] S. Ossokine,[112] C. Osthelder,[1] S. Otabe,[2] D. J. Ottaway,[89] H. Overmier,[57] A. E. Pace,[150] G. Pagano,[79,18] R. Pagano,[7] M. A. Page,[94] G. Pagliaroli,[32,108] A. Pai,[107] S. A. Pai,[95] S. Pal,[246] J. R. Palamos,[67] O. Palashov,[215] C. Palomba,[58] H. Pan,[130] K.-C. Pan,[138,195] P. K. Panda,[203] P. T. H. Pang,[60,66] C. Pankow,[15] F. Pannarale,[105,58] B. C. Pant,[95] F. H. Panther,[94] F. Paoletti,[18] A. Paoli,[47] A. Paolone,[58,249] G. Pappas,[200] A. Parisi,[134] H. Park,[6] J. Park,[250] W. Parker,[57] D. Pascucci,[60,86] A. Pasqualetti,[47] R. Passaquieti,[79,18] D. Passuello,[18] M. Patel,[64] M. Pathak,[89] B. Patricelli,[47,18] A. S. Patron,[7] S. Paul,[67] E. Payne,[5] M. Pedraza,[1] R. Pedurand,[104] M. Pegoraro,[82] A. Pele,[57] F. E. Peña Arellano,[190] S. Penano,[78] S. Penn,[251] A. Perego,[99,100] A. Pereira,[26]

T. Pereira,[252] C. J. Perez,[73] C. Périgois,[30] C. C. Perkins,[77] A. Perreca,[99,100] S. Perriès,[141] D. Pesios,[200] J. Petermann,[128] D. Petterson,[1] H. P. Pfeiffer,[112] H. Pham,[57] K. A. Pham,[149] K. S. Phukon,[60,212] H. Phurailatpam,[131] O. J. Piccinni,[58] M. Pichot,[37] M. Piendibene,[79,18] F. Piergiovanni,[55,56] L. Pierini,[105,58] V. Pierro,[88,104] G. Pillant,[47] M. Pillas,[46] F. Pilo,[18] L. Pinard,[157] C. Pineda-Bosque,[91] I. M. Pinto,[88,104,253] M. Pinto,[47] B. J. Piotrzkowski,[6] K. Piotrzkowski,[59] M. Pirello,[73] M. D. Pitkin,[193] A. Placidi,[40,80] E. Placidi,[105,58] M. L. Planas,[145] W. Plastino,[254,235] C. Pluchar,[255] R. Poggiani,[79,18] E. Polini,[30] D. Y. T. Pong,[131] S. Ponrathnam,[11] E. K. Porter,[45] R. Poulton,[47] A. Poverman,[83] J. Powell,[143] M. Pracchia,[30] T. Pradier,[164] A. K. Prajapati,[85] K. Prasai,[78] R. Prasanna,[203] G. Pratten,[14] M. Principe,[88,253,104] G. A. Prodi,[256,100] L. Prokhorov,[14] P. Prosposito,[124,125] L. Prudenzi,[112] A. Puecher,[60,66] M. Punturo,[40] F. Puosi,[18,79] P. Puppo,[58] M. Pürrer,[112] H. Qi,[17] N. Quartey,[64] V. Quetschke,[90] P. J. Quinonez,[36] R. Quitzow-James,[96] F. J. Raab,[73] G. Raaijmakers,[38,60] H. Radkins,[73] N. Radulesco,[37] P. Raffai,[154] S. X. Rail,[224] S. Raja,[95] C. Rajan,[95] K. E. Ramirez,[57] T. D. Ramirez,[44] A. Ramos-Buades,[112] J. Rana,[150] P. Rapagnani,[105,58] A. Ray,[6] V. Raymond,[17] N. Raza,[181] M. Razzano,[79,18] J. Read,[44] L. A. Rees,[42] T. Regimbau,[30] L. Rei,[93] S. Reid,[33] S. W. Reid,[64] D. H. Reitze,[1,77] P. Relton,[17] A. Renzini,[1] P. Rettegno,[22,23] B. Revenu,[45] A. Reza,[60] M. Rezac,[44] F. Ricci,[105,58] D. Richards,[196] J. W. Richardson,[257] L. Richardson,[185] G. Riemenschneider,[22,23] K. Riles,[184] S. Rinaldi,[79,18] K. Rink,[181] N. A. Robertson,[1] R. Robie,[1] F. Robinet,[46] A. Rocchi,[125] S. Rodriguez,[44] L. Rolland,[30] J. G. Rollins,[1] M. Romanelli,[106] R. Romano,[3,4] C. L. Romel,[73] A. Romero,[31] I. M. Romero-Shaw,[5] J. H. Romie,[57] S. Ronchini,[32,108] L. Rosa,[4,25] C. A. Rose,[6] D. Rosińska,[110] M. P. Ross,[258] S. Rowan,[24] S. J. Rowlinson,[14] S. Roy,[66] Santosh Roy,[11] Soumen Roy,[259] D. Rozza,[122,123] P. Ruggi,[47] K. Ruiz-Rocha,[204] K. Ryan,[73] S. Sachdev,[150] T. Sadecki,[73] J. Sadiq,[115] S. Saha,[195] Y. Saito,[190] K. Sakai,[260] M. Sakellariadou,[61] S. Sakon,[150] O. S. Salafia,[72,71,70] F. Salces-Carcoba,[1] L. Salconi,[47] M. Saleem,[149] F. Salemi,[99,100] A. Samajdar,[71] E. J. Sanchez,[1] J. H. Sanchez,[44] L. E. Sanchez,[1] N. Sanchis-Gual,[261] J. R. Sanders,[262] A. Sanuy,[29] T. R. Saravanan,[11] N. Sarin,[5] B. Sassolas,[157] H. Satari,[94] O. Sauter,[77] R. L. Savage,[73] V. Savant,[11] T. Sawada,[177] H. L. Sawant,[11] S. Sayah,[157] D. Schaetzl,[1] M. Scheel,[137] J. Scheuer,[15] M. G. Schiworski,[89] P. Schmidt,[14] S. Schmidt,[66] R. Schnabel,[128] M. Schneewind,[9,10] R. M. S. Schofield,[67] A. Schönbeck,[128] B. W. Schulte,[9,10] B. F. Schutz,[17,9,10] E. Schwartz,[17] J. Scott,[24] S. M. Scott,[8] M. Seglar-Arroyo,[30] Y. Sekiguchi,[263] D. Sellers,[57] A. S. Sengupta,[259] D. Sentenac,[47] E. G. Seo,[131] V. Sequino,[25,4] A. Sergeev,[215] Y. Setyawati,[9,10,66] T. Shaffer,[73] M. S. Shahriar,[15] M. A. Shaikh,[19] B. Shams,[160] L. Shao,[199] A. Sharma,[32,108] P. Sharma,[95] P. Shawhan,[111] N. S. Shcheblanov,[228] A. Sheela,[241] Y. Shikano,[264,265] M. Shikauchi,[28] H. Shimizu,[266] K. Shimode,[190] H. Shinkai,[267] T. Shishido,[54] A. Shoda,[20] D. H. Shoemaker,[75] D. M. Shoemaker,[170] S. ShyamSundar,[95] M. Sieniawska,[59] D. Sigg,[73] L. Silenzi,[40,41] L. P. Singer,[118] D. Singh,[150] M. K. Singh,[19] N. Singh,[110] A. Singha,[155,60] A. M. Sintes,[145] V. Sipala,[122,123] V. Skliris,[17] B. J. J. Slagmolen,[8] T. J. Slaven-Blair,[94] J. Smetana,[14] J. R. Smith,[44] L. Smith,[24] R. J. E. Smith,[5] J. Soldateschi,[229,268,56] S. N. Somala,[269] K. Somiya,[2] I. Song,[195] K. Soni,[11] V. Sordini,[141] F. Sorrentino,[93] N. Sorrentino,[79,18] R. Soulard,[37] T. Souradeep,[270,11] E. Sowell,[148] V. Spagnuolo,[155,60] A. P. Spencer,[24] M. Spera,[81,82] P. Spinicelli,[47] A. K. Srivastava,[85] V. Srivastava,[68] K. Staats,[15] C. Stachie,[37] F. Stachurski,[24] D. A. Steer,[45] J. Steinlechner,[155,60] S. Steinlechner,[155,60] N. Stergioulas,[200] D. J. Stops,[14] M. Stover,[237] K. A. Strain,[24] L. C. Strang,[121] G. Stratta,[271,58] M. D. Strong,[7] A. Strunk,[73] R. Sturani,[252] A. L. Stuver,[114] M. Suchenek,[87] S. Sudhagar,[11] V. Sudhir,[75] R. Sugimoto,[272,243] H. G. Suh,[6] A. G. Sullivan,[51] T. Z. Summerscales,[273] L. Sun,[8] S. Sunil,[85] A. Sur,[87] J. Suresh,[28] P. J. Sutton,[17] Takamasa Suzuki,[176] Takanori Suzuki,[2] Toshikazu Suzuki,[188] B. L. Swinkels,[60] M. J. Szczepańczyk,[77] P. Szewczyk,[110] M. Tacca,[60] H. Tagoshi,[188] S. C. Tait,[24] H. Takahashi,[274] R. Takahashi,[20] S. Takano,[27] H. Takeda,[27] M. Takeda,[177] C. J. Talbot,[33] C. Talbot,[1] K. Tanaka,[275] Taiki Tanaka,[188] Takahiro Tanaka,[276] A. J. Tanasijczuk,[59] S. Tanioka,[190] D. B. Tanner,[77] D. Tao,[1] L. Tao,[77] R. D. Tapia,[150] E. N. Tapia San Martín,[60] C. Taranto,[124] A. Taruya,[277] J. D. Tasson,[161] R. Tenorio,[145] J. E. S. Terhune,[114] L. Terkowski,[128] M. P. Thirugnanasambandam,[11] M. Thomas,[57] P. Thomas,[73] E. E. Thompson,[48] J. E. Thompson,[17] S. R. Thondapu,[95] K. A. Thorne,[57] E. Thrane,[5] Shubhanshu Tiwari,[162] Srishti Tiwari,[11] V. Tiwari,[17] A. M. Toivonen,[149] A. E. Tolley,[52] T. Tomaru,[20] T. Tomura,[190] M. Tonelli,[79,18] Z. Tornasi,[24] A. Torres-Forné,[127] C. I. Torrie,[1] I. Tosta e Melo,[123] D. Töyrä,[8] A. Trapananti,[41,40] F. Travasso,[40,41] G. Traylor,[57] M. Trevor,[111] M. C. Tringali,[47] A. Tripathee,[184] L. Troiano,[278,104] A. Trovato,[45] L. Trozzo,[4,190] R. J. Trudeau,[1] D. Tsai,[130] K. W. Tsang,[60,279,66] T. Tsang,[280] J-S. Tsao,[233] M. Tse,[75] R. Tso,[137] S. Tsuchida,[177] L. Tsukada,[150] D. Tsuna,[28] T. Tsutsui,[28] K. Turbang,[281,205] M. Turconi,[37] D. Tuyenbayev,[177] A. S. Ubhi,[14] N. Uchikata,[188] T. Uchiyama,[190] R. P. Udall,[1] A. Ueda,[282] T. Uehara,[283,284] K. Ueno,[28] G. Ueshima,[285] C. S. Unnikrishnan,[286] A. L. Urban,[7] T. Ushiba,[190] A. Utina,[155,60] G. Vajente,[1] A. Vajpeyi,[5] G. Valdes,[185] M. Valentini,[183,99,100] V. Valsan,[6] N. van Bakel,[60] M. van Beuzekom,[60] M. van Dael,[60,287] J. F. J. van den Brand,[155,97,60] C. Van Den Broeck,[66,60] D. C. Vander-Hyde,[68] H. van Haevermaet,[205] J. V. van Heijningen,[59] M. H. P. M. van Putten,[288]

N. van Remortel,[205] M. Vardaro,[212,60] A. F. Vargas,[121] V. Varma,[112] M. Vasúth,[76] A. Vecchio,[14] G. Vedovato,[82] J. Veitch,[24] P. J. Veitch,[89] J. Venneberg,[9,10] G. Venugopalan,[1] D. Verkindt,[30] P. Verma,[221] Y. Verma,[95] S. M. Vermeulen,[17] D. Veske,[51] F. Vetrano,[55] A. Viceré,[55,56] S. Vidyant,[68] A. D. Viets,[289] A. Vijaykumar,[19] V. Villa-Ortega,[115] J.-Y. Vinet,[37] A. Virtuoso,[239,35] S. Vitale,[75] H. Vocca,[80,40] E. R. G. von Reis,[73] J. S. A. von Wrangel,[9,10] C. Vorvick,[73] S. P. Vyatchanin,[98] L. E. Wade,[237] M. Wade,[237] K. J. Wagner,[129] R. C. Walet,[60] M. Walker,[64] G. S. Wallace,[33] L. Wallace,[1] J. Wang,[178] J. Z. Wang,[184] W. H. Wang,[90] R. L. Ward,[8] J. Warner,[73] M. Was,[30] T. Washimi,[20] N. Y. Washington,[1] J. Watchi,[146] B. Weaver,[73] C. R. Weaving,[52] S. A. Webster,[24] M. Weinert,[9,10] A. J. Weinstein,[1] R. Weiss,[75] C. M. Weller,[258] R. A. Weller,[204] F. Wellmann,[9,10] L. Wen,[94] P. Weßels,[9,10] K. Wette,[8] J. T. Whelan,[129] D. D. White,[44] B. F. Whiting,[77] C. Whittle,[75] D. Wilken,[9,10] D. Williams,[24] M. J. Williams,[24] A. R. Williamson,[52] J. L. Willis,[1] B. Willke,[9,10] D. J. Wilson,[255] C. C. Wipf,[1] T. Wlodarczyk,[112] G. Woan,[24] J. Woehler,[9,10] J. K. Wofford,[129] D. Wong,[181] I. C. F. Wong,[131] M. Wright,[24] C. Wu,[138] D. S. Wu,[9,10] H. Wu,[138] D. M. Wysocki,[6] L. Xiao,[1] T. Yamada,[266] H. Yamamoto,[1] K. Yamamoto,[189] T. Yamamoto,[190] K. Yamashita,[201] R. Yamazaki,[198] F. W. Yang,[160] K. Z. Yang,[149] L. Yang,[168] Y.-C. Yang,[130] Y. Yang,[290] Yang Yang,[77] M. J. Yap,[8] D. W. Yeeles,[17] S.-W. Yeh,[138] A. B. Yelikar,[129] M. Ying,[130] J. Yokoyama,[28,27] T. Yokozawa,[190] J. Yoo,[180] T. Yoshioka,[201] Hang Yu,[137] Haocun Yu,[75] H. Yuzurihara,[188] A. Zadrożny,[221] M. Zanolin,[36] S. Zeidler,[291] T. Zelenova,[47] J.-P. Zendri,[82] M. Zevin,[166] M. Zhan,[178] H. Zhang,[233] J. Zhang,[94] L. Zhang,[1] R. Zhang,[77] T. Zhang,[14] Y. Zhang,[185] C. Zhao,[94] G. Zhao,[146] Y. Zhao,[188,20] Yue Zhao,[160] R. Zhou,[191] Z. Zhou,[15] X. J. Zhu,[5] Z.-H. Zhu,[120,231] A. B. Zimmerman,[170] M. E. Zucker,[1,75] and J. Zweizig[1]

(The LIGO Scientific Collaboration, the Virgo Collaboration, and the KAGRA Collaboration)

[1]*LIGO Laboratory, California Institute of Technology, Pasadena, California 91125, USA*
[2]*Graduate School of Science, Tokyo Institute of Technology, Meguro-ku, Tokyo 152-8551, Japan*
[3]*Dipartimento di Farmacia, Università di Salerno, I-84084 Fisciano, Salerno, Italy*
[4]*INFN, Sezione di Napoli, Complesso Universitario di Monte S. Angelo, I-80126 Napoli, Italy*
[5]*OzGrav, School of Physics and Astronomy, Monash University, Clayton 3800, Victoria, Australia*
[6]*University of Wisconsin-Milwaukee, Milwaukee, Wisconsin 53201, USA*
[7]*Louisiana State University, Baton Rouge, Louisiana 70803, USA*
[8]*OzGrav, Australian National University, Canberra, Australian Capital Territory 0200, Australia*
[9]*Max Planck Institute for Gravitational Physics (Albert Einstein Institute), D-30167 Hannover, Germany*
[10]*Leibniz Universität Hannover, D-30167 Hannover, Germany*
[11]*Inter-University Centre for Astronomy and Astrophysics, Pune 411007, India*
[12]*University of Cambridge, Cambridge CB2 1TN, United Kingdom*
[13]*Theoretisch-Physikalisches Institut, Friedrich-Schiller-Universität Jena, D-07743 Jena, Germany*
[14]*University of Birmingham, Birmingham B15 2TT, United Kingdom*
[15]*Northwestern University, Evanston, Illinois 60208, USA*
[16]*Instituto Nacional de Pesquisas Espaciais, 12227-010 São José dos Campos, São Paulo, Brazil*
[17]*Cardiff University, Cardiff CF24 3AA, United Kingdom*
[18]*INFN, Sezione di Pisa, I-56127 Pisa, Italy*
[19]*International Centre for Theoretical Sciences, Tata Institute of Fundamental Research, Bengaluru 560089, India*
[20]*Gravitational Wave Science Project, National Astronomical Observatory of Japan (NAOJ), Mitaka City, Tokyo 181-8588, Japan*
[21]*Advanced Technology Center, National Astronomical Observatory of Japan (NAOJ), Mitaka City, Tokyo 181-8588, Japan*
[22]*Dipartimento di Fisica, Università degli Studi di Torino, I-10125 Torino, Italy*
[23]*INFN Sezione di Torino, I-10125 Torino, Italy*
[24]*SUPA, University of Glasgow, Glasgow G12 8QQ, United Kingdom*
[25]*Università di Napoli "Federico II", Complesso Universitario di Monte S. Angelo, I-80126 Napoli, Italy*
[26]*Université de Lyon, Université Claude Bernard Lyon 1, CNRS, Institut Lumière Matière, F-69622 Villeurbanne, France*
[27]*Department of Physics, The University of Tokyo, Bunkyo-ku, Tokyo 113-0033, Japan*
[28]*Research Center for the Early Universe (RESCEU), The University of Tokyo, Bunkyo-ku, Tokyo 113-0033, Japan*
[29]*Institut de Ciències del Cosmos (ICCUB), Universitat de Barcelona, C/ Martí i Franquès 1, Barcelona 08028, Spain*

[30]Université Savoie Mont Blanc, CNRS, Laboratoire d'Annecy de Physique des Particules—IN2P3, F-74000 Annecy, France
[31]Institut de Física d'Altes Energies (IFAE), Barcelona Institute of Science and Technology, and ICREA, E-08193 Barcelona, Spain
[32]Gran Sasso Science Institute (GSSI), I-67100 L'Aquila, Italy
[33]SUPA, University of Strathclyde, Glasgow G1 1XQ, United Kingdom
[34]Dipartimento di Scienze Matematiche, Informatiche e Fisiche, Università di Udine, I-33100 Udine, Italy
[35]INFN, Sezione di Trieste, I-34127 Trieste, Italy
[36]Embry-Riddle Aeronautical University, Prescott, Arizona 86301, USA
[37]Artemis, Université Côte d'Azur, Observatoire de la Côte d'Azur, CNRS, F-06304 Nice, France
[38]GRAPPA, Anton Pannekoek Institute for Astronomy and Institute for High-Energy Physics, University of Amsterdam, Science Park 904, 1098 XH Amsterdam, Netherlands
[39]National and Kapodistrian University of Athens, School of Science Building, 2nd floor, Panepistimiopolis, 15771 Ilissia, Greece
[40]INFN, Sezione di Perugia, I-06123 Perugia, Italy
[41]Università di Camerino, Dipartimento di Fisica, I-62032 Camerino, Italy
[42]American University, Washington, DC 20016, USA
[43]Earthquake Research Institute, The University of Tokyo, Bunkyo-ku, Tokyo 113-0032, Japan
[44]California State University Fullerton, Fullerton, California 92831, USA
[45]Université de Paris, CNRS, Astroparticule et Cosmologie, F-75006 Paris, France
[46]Université Paris-Saclay, CNRS/IN2P3, IJCLab, 91405 Orsay, France
[47]European Gravitational Observatory (EGO), I-56021 Cascina, Pisa, Italy
[48]Georgia Institute of Technology, Atlanta, Georgia 30332, USA
[49]Chennai Mathematical Institute, Chennai 603103, India
[50]Department of Mathematics and Physics, Hirosaki University, 036-8560 Aomori, Hirosaki, Bunkyocho, 1, Japan
[51]Columbia University, New York, New York 10027, USA
[52]University of Portsmouth, Portsmouth PO1 3FX, United Kingdom
[53]Kamioka Branch, National Astronomical Observatory of Japan (NAOJ), Kamioka-cho, Hida City, Gifu 506-1205, Japan
[54]The Graduate University for Advanced Studies (SOKENDAI), Mitaka City, Tokyo 181-8588, Japan
[55]Università degli Studi di Urbino "Carlo Bo", I-61029 Urbino, Italy
[56]INFN, Sezione di Firenze, I-50019 Sesto Fiorentino, Firenze, Italy
[57]LIGO Livingston Observatory, Livingston, Louisiana 70754, USA
[58]INFN, Sezione di Roma, I-00185 Roma, Italy
[59]Université catholique de Louvain, B-1348 Louvain-la-Neuve, Belgium
[60]Nikhef, Science Park 105, 1098 XG Amsterdam, Netherlands
[61]King's College London, University of London, London WC2R 2LS, United Kingdom
[62]Korea Institute of Science and Technology Information, Daejeon 34141, Republic of Korea
[63]National Institute for Mathematical Sciences, Daejeon 34047, Republic of Korea
[64]Christopher Newport University, Newport News, Virginia 23606, USA
[65]School of High Energy Accelerator Science, The Graduate University for Advanced Studies (SOKENDAI), Tsukuba City, Ibaraki 305-0801, Japan
[66]Institute for Gravitational and Subatomic Physics (GRASP), Utrecht University, Princetonplein 1, 3584 CC Utrecht, Netherlands
[67]University of Oregon, Eugene, Oregon 97403, USA
[68]Syracuse University, Syracuse, New York 13244, USA
[69]Université de Liège, B-4000 Liège, Belgium
[70]Università degli Studi di Milano-Bicocca, I-20126 Milano, Italy
[71]INFN, Sezione di Milano-Bicocca, I-20126 Milano, Italy
[72]INAF, Osservatorio Astronomico di Brera sede di Merate, I-23807 Merate, Lecco, Italy
[73]LIGO Hanford Observatory, Richland, Washington 99352, USA
[74]Dipartimento di Medicina, Chirurgia e Odontoiatria "Scuola Medica Salernitana," Università di Salerno, I-84081 Baronissi, Salerno, Italy
[75]LIGO Laboratory, Massachusetts Institute of Technology, Cambridge, Massachusetts 02139, USA
[76]Wigner RCP, RMKI, H-1121 Budapest, Konkoly Thege Miklós út 29-33, Hungary
[77]University of Florida, Gainesville, Florida 32611, USA
[78]Stanford University, Stanford, California 94305, USA
[79]Università di Pisa, I-56127 Pisa, Italy
[80]Università di Perugia, I-06123 Perugia, Italy

[81]*Università di Padova, Dipartimento di Fisica e Astronomia, I-35131 Padova, Italy*
[82]*INFN, Sezione di Padova, I-35131 Padova, Italy*
[83]*Bard College, Annandale-On-Hudson, New York 12504, USA*
[84]*Montana State University, Bozeman, Montana 59717, USA*
[85]*Institute for Plasma Research, Bhat, Gandhinagar 382428, India*
[86]*Universiteit Gent, B-9000 Gent, Belgium*
[87]*Nicolaus Copernicus Astronomical Center, Polish Academy of Sciences, 00-716 Warsaw, Poland*
[88]*Dipartimento di Ingegneria, Università del Sannio, I-82100 Benevento, Italy*
[89]*OzGrav, University of Adelaide, Adelaide, South Australia 5005, Australia*
[90]*The University of Texas Rio Grande Valley, Brownsville, Texas 78520, USA*
[91]*California State University, Los Angeles, Los Angeles, California 90032, USA*
[92]*Departamento de Matemáticas, Universitat Autònoma de Barcelona, Edificio C Facultad de Ciencias, 08193 Bellaterra (Barcelona), Spain*
[93]*INFN, Sezione di Genova, I-16146 Genova, Italy*
[94]*OzGrav, University of Western Australia, Crawley, Western Australia 6009, Australia*
[95]*RRCAT, Indore, Madhya Pradesh 452013, India*
[96]*Missouri University of Science and Technology, Rolla, Missouri 65409, USA*
[97]*Vrije Universiteit Amsterdam, 1081 HV Amsterdam, Netherlands*
[98]*Lomonosov Moscow State University, Moscow 119991, Russia*
[99]*Università di Trento, Dipartimento di Fisica, I-38123 Povo, Trento, Italy*
[100]*INFN, Trento Institute for Fundamental Physics and Applications, I-38123 Povo, Trento, Italy*
[101]*SUPA, University of the West of Scotland, Paisley PA1 2BE, United Kingdom*
[102]*Bar-Ilan University, Ramat Gan, 5290002, Israel*
[103]*Dipartimento di Fisica "E.R. Caianiello," Università di Salerno, I-84084 Fisciano, Salerno, Italy*
[104]*INFN, Sezione di Napoli, Gruppo Collegato di Salerno, Complesso Universitario di Monte S. Angelo, I-80126 Napoli, Italy*
[105]*Università di Roma "La Sapienza", I-00185 Roma, Italy*
[106]*Univ Rennes, CNRS, Institut FOTON—UMR6082, F-3500 Rennes, France*
[107]*Indian Institute of Technology Bombay, Powai, Mumbai 400 076, India*
[108]*INFN, Laboratori Nazionali del Gran Sasso, I-67100 Assergi, Italy*
[109]*Laboratoire Kastler Brossel, Sorbonne Université, CNRS, ENS-Université PSL, Collège de France, F-75005 Paris, France*
[110]*Astronomical Observatory Warsaw University, 00-478 Warsaw, Poland*
[111]*University of Maryland, College Park, Maryland 20742, USA*
[112]*Max Planck Institute for Gravitational Physics (Albert Einstein Institute), D-14476 Potsdam, Germany*
[113]*L2IT, Laboratoire des 2 Infinis—Toulouse, Université de Toulouse, CNRS/IN2P3, UPS, F-31062 Toulouse Cedex 9, France*
[114]*Villanova University, Villanova, Pennsylvania 19085, USA*
[115]*IGFAE, Universidade de Santiago de Compostela, Santiago de Compostela 15782, Spain*
[116]*Stony Brook University, Stony Brook, New York 11794, USA*
[117]*Center for Computational Astrophysics, Flatiron Institute, New York, New York 10010, USA*
[118]*NASA Goddard Space Flight Center, Greenbelt, Maryland 20771, USA*
[119]*Dipartimento di Fisica, Università degli Studi di Genova, I-16146 Genova, Italy*
[120]*Department of Astronomy, Beijing Normal University, Beijing 100875, China*
[121]*OzGrav, University of Melbourne, Parkville, Victoria 3010, Australia*
[122]*Università degli Studi di Sassari, I-07100 Sassari, Italy*
[123]*INFN, Laboratori Nazionali del Sud, I-95125 Catania, Italy*
[124]*Università di Roma Tor Vergata, I-00133 Roma, Italy*
[125]*INFN, Sezione di Roma Tor Vergata, I-00133 Roma, Italy*
[126]*University of Sannio at Benevento, I-82100 Benevento, Italy and INFN, Sezione di Napoli, I-80100 Napoli, Italy*
[127]*Departamento de Astronomía y Astrofísica, Universitat de València, E-46100 Burjassot, València, Spain*
[128]*Universität Hamburg, D-22761 Hamburg, Germany*
[129]*Rochester Institute of Technology, Rochester, New York 14623, USA*
[130]*National Tsing Hua University, Hsinchu City, 30013 Taiwan, Republic of China*
[131]*The Chinese University of Hong Kong, Shatin, NT, Hong Kong*
[132]*Department of Applied Physics, Fukuoka University, Jonan, Fukuoka City, Fukuoka 814-0180, Japan*
[133]*OzGrav, Charles Sturt University, Wagga Wagga, New South Wales 2678, Australia*
[134]*Department of Physics, Tamkang University, Danshui District, New Taipei City 25137, Taiwan*

[135]Department of Physics and Institute of Astronomy, National Tsing Hua University, Hsinchu 30013, Taiwan
[136]Department of Physics, Center for High Energy and High Field Physics, National Central University, Zhongli District, Taoyuan City 32001, Taiwan
[137]CaRT, California Institute of Technology, Pasadena, California 91125, USA
[138]Department of Physics, National Tsing Hua University, Hsinchu 30013, Taiwan
[139]Dipartimento di Ingegneria Industriale (DIIN), Università di Salerno, I-84084 Fisciano, Salerno, Italy
[140]Institute of Physics, Academia Sinica, Nankang, Taipei 11529, Taiwan
[141]Université Lyon, Université Claude Bernard Lyon 1, CNRS, IP2I Lyon / IN2P3, UMR 5822, F-69622 Villeurbanne, France
[142]INAF, Osservatorio Astronomico di Padova, I-35122 Padova, Italy
[143]OzGrav, Swinburne University of Technology, Hawthorn VIC 3122, Australia
[144]Université libre de Bruxelles, Avenue Franklin Roosevelt, 50–1050 Bruxelles, Belgium
[145]IAC3–IEEC, Universitat de les Illes Balears, E-07122 Palma de Mallorca, Spain
[146]Université Libre de Bruxelles, Brussels 1050, Belgium
[147]Departamento de Matemáticas, Universitat de València, E-46100 Burjassot, València, Spain
[148]Texas Tech University, Lubbock, Texas 79409, USA
[149]University of Minnesota, Minneapolis, Minnesota 55455, USA
[150]The Pennsylvania State University, University Park, Pennsylvania 16802, USA
[151]University of Rhode Island, Kingston, Rhode Island 02881, USA
[152]Bellevue College, Bellevue, Washington 98007, USA
[153]Scuola Normale Superiore, Piazza dei Cavalieri, 7–56126 Pisa, Italy
[154]Eötvös University, Budapest 1117, Hungary
[155]Maastricht University, P.O. Box 616, 6200 MD Maastricht, Netherlands
[156]The University of Sheffield, Sheffield S10 2TN, United Kingdom
[157]Université Lyon, Université Claude Bernard Lyon 1, CNRS, Laboratoire des Matériaux Avancés (LMA), IP2I Lyon / IN2P3, UMR 5822, F-69622 Villeurbanne, France
[158]Dipartimento di Scienze Matematiche, Fisiche e Informatiche, Università di Parma, I-43124 Parma, Italy
[159]INFN, Sezione di Milano Bicocca, Gruppo Collegato di Parma, I-43124 Parma, Italy
[160]The University of Utah, Salt Lake City, Utah 84112, USA
[161]Carleton College, Northfield, Minnesota 55057, USA
[162]University of Zurich, Winterthurerstrasse 190, 8057 Zurich, Switzerland
[163]Perimeter Institute, Waterloo, Ontario N2L 2Y5, Canada
[164]Université de Strasbourg, CNRS, IPHC UMR 7178, F-67000 Strasbourg, France
[165]West Virginia University, Morgantown, West Virginia 26506, USA
[166]University of Chicago, Chicago, Illinois 60637, USA
[167]Montclair State University, Montclair, New Jersey 07043, USA
[168]Colorado State University, Fort Collins, Colorado 80523, USA
[169]Institute for Nuclear Research, Bem t'er 18/c, H-4026 Debrecen, Hungary
[170]University of Texas, Austin, Texas 78712, USA
[171]CNR-SPIN, c/o Università di Salerno, I-84084 Fisciano, Salerno, Italy
[172]Scuola di Ingegneria, Università della Basilicata, I-85100 Potenza, Italy
[173]Observatori Astronòmic, Universitat de València, E-46980 Paterna, València, Spain
[174]Centro de Física das Universidades do Minho e do Porto, Universidade do Minho, Campus de Gualtar, PT-4710–057 Braga, Portugal
[175]Department of Astronomy, The University of Tokyo, Mitaka City, Tokyo 181-8588, Japan
[176]Faculty of Engineering, Niigata University, Nishi-ku, Niigata City, Niigata 950-2181, Japan
[177]Department of Physics, Graduate School of Science, Osaka City University, Sumiyoshi-ku, Osaka City, Osaka 558-8585, Japan
[178]State Key Laboratory of Magnetic Resonance and Atomic and Molecular Physics, Innovation Academy for Precision Measurement Science and Technology (APM), Chinese Academy of Sciences, Xiao Hong Shan, Wuhan 430071, China
[179]University of Szeged, Dóm tér 9, Szeged 6720, Hungary
[180]Cornell University, Ithaca, New York 14850, USA
[181]University of British Columbia, Vancouver, British Columbia V6T 1Z4, Canada
[182]INAF, Osservatorio Astronomico di Capodimonte, I-80131 Napoli, Italy
[183]The University of Mississippi, University, Mississippi 38677, USA
[184]University of Michigan, Ann Arbor, Michigan 48109, USA
[185]Texas A&M University, College Station, Texas 77843, USA

[186]*Ulsan National Institute of Science and Technology, Ulsan 44919, Republic of Korea*
[187]*Shanghai Astronomical Observatory, Chinese Academy of Sciences, Shanghai 200030, China*
[188]*Institute for Cosmic Ray Research (ICRR), KAGRA Observatory, The University of Tokyo, Kashiwa City, Chiba 277-8582, Japan*
[189]*Faculty of Science, University of Toyama, Toyama City, Toyama 930-8555, Japan*
[190]*Institute for Cosmic Ray Research (ICRR), KAGRA Observatory, The University of Tokyo, Kamioka-cho, Hida City, Gifu 506-1205, Japan*
[191]*University of California, Berkeley, California 94720, USA*
[192]*Maastricht University, 6200 MD Maastricht, Netherlands*
[193]*Lancaster University, Lancaster LA1 4YW, United Kingdom*
[194]*College of Industrial Technology, Nihon University, Narashino City, Chiba 275-8575, Japan*
[195]*Institute of Astronomy, National Tsing Hua University, Hsinchu 30013, Taiwan*
[196]*Rutherford Appleton Laboratory, Didcot OX11 0DE, United Kingdom*
[197]*Department of Astronomy and Space Science, Chungnam National University, Yuseong-gu, Daejeon 34134, Republic of Korea*
[198]*Department of Physical Sciences, Aoyama Gakuin University, Sagamihara City, Kanagawa 252-5258, Japan*
[199]*Kavli Institute for Astronomy and Astrophysics, Peking University, Haidian District, Beijing 100871, China*
[200]*Aristotle University of Thessaloniki, University Campus, 54124 Thessaloniki, Greece*
[201]*Graduate School of Science and Engineering, University of Toyama, Toyama City, Toyama 930-8555, Japan*
[202]*Nambu Yoichiro Institute of Theoretical and Experimental Physics (NITEP), Osaka City University, Sumiyoshi-ku, Osaka City, Osaka 558-8585, Japan*
[203]*Directorate of Construction, Services and Estate Management, Mumbai 400094, India*
[204]*Vanderbilt University, Nashville, Tennessee 37235, USA*
[205]*Universiteit Antwerpen, Prinsstraat 13, 2000 Antwerpen, Belgium*
[206]*University of Białystok, 15-424 Białystok, Poland*
[207]*Ewha Womans University, Seoul 03760, Republic of Korea*
[208]*National Astronomical Observatories, Chinese Academic of Sciences, Chaoyang District, Beijing 100107, China*
[209]*School of Astronomy and Space Science, University of Chinese Academy of Sciences, Chaoyang District, Beijing 100107, China*
[210]*University of Southampton, Southampton SO17 1BJ, United Kingdom*
[211]*Institute for Cosmic Ray Research (ICRR), The University of Tokyo, Kashiwa City, Chiba 277-8582, Japan*
[212]*Institute for High-Energy Physics, University of Amsterdam, Science Park 904, 1098 XH Amsterdam, Netherlands*
[213]*Chung-Ang University, Seoul 06974, Republic of Korea*
[214]*University of Washington Bothell, Bothell, Washington 98011, USA*
[215]*Institute of Applied Physics, Nizhny Novgorod 603950, Russia*
[216]*Inje University Gimhae, South Gyeongsang 50834, Republic of Korea*
[217]*Department of Physics, Myongji University, Yongin 17058, Republic of Korea*
[218]*Institute of Particle and Nuclear Studies (IPNS), High Energy Accelerator Research Organization (KEK), Tsukuba City, Ibaraki 305-0801, Japan*
[219]*School of Physics and Astronomy, Cardiff University, Cardiff CF24 3AA, United Kingdom*
[220]*Institute of Mathematics, Polish Academy of Sciences, 00656 Warsaw, Poland*
[221]*National Center for Nuclear Research, 05-400 Świerk-Otwock, Poland*
[222]*Instituto de Fisica Teorica, 28049 Madrid, Spain*
[223]*Department of Physics, Nagoya University, Chikusa-ku, Nagoya, Aichi 464-8602, Japan*
[224]*Université de Montréal/Polytechnique, Montreal, Quebec H3T 1J4, Canada*
[225]*Laboratoire Lagrange, Université Côte d'Azur, Observatoire Côte d'Azur, CNRS, F-06304 Nice, France*
[226]*Seoul National University, Seoul 08826, Republic of Korea*
[227]*Sungkyunkwan University, Seoul 03063, Republic of Korea*
[228]*NAVIER, École des Ponts, Univ Gustave Eiffel, CNRS, Marne-la-Vallée 77420, France*
[229]*Università di Firenze, Sesto Fiorentino I-50019, Italy*
[230]*Department of Physics, National Cheng Kung University, Tainan City 701, Taiwan*
[231]*School of Physics and Technology, Wuhan University, Wuhan, Hubei 430072, China*

[232]National Center for High-performance computing, National Applied Research Laboratories, Hsinchu Science Park, Hsinchu City 30076, Taiwan
[233]Department of Physics, National Taiwan Normal University, sec. IV, Taipei 116, Taiwan
[234]NASA Marshall Space Flight Center, Huntsville, Alabama 35811, USA
[235]INFN, Sezione di Roma Tre, I-00146 Roma, Italy
[236]ESPCI, CNRS, F-75005 Paris, France
[237]Kenyon College, Gambier, Ohio 43022, USA
[238]School of Physics Science and Engineering, Tongji University, Shanghai 200092, China
[239]Dipartimento di Fisica, Università di Trieste, I-34127 Trieste, Italy
[240]Institute for Photon Science and Technology, The University of Tokyo, Bunkyo-ku, Tokyo 113-8656, Japan
[241]Indian Institute of Technology Madras, Chennai 600036, India
[242]Saha Institute of Nuclear Physics, Bidhannagar, West Bengal 700064, India
[243]Institute of Space and Astronautical Science (JAXA), Chuo-ku, Sagamihara City, Kanagawa 252-0222, Japan
[244]Institut des Hautes Etudes Scientifiques, F-91440 Bures-sur-Yvette, France
[245]Faculty of Law, Ryukoku University, Fushimi-ku, Kyoto City, Kyoto 612-8577, Japan
[246]Indian Institute of Science Education and Research, Kolkata, Mohanpur, West Bengal 741252, India
[247]Department of Physics, University of Notre Dame, Notre Dame, Indiana 46556, USA
[248]Graduate School of Science and Technology, Niigata University, Nishi-ku, Niigata City, Niigata 950-2181, Japan
[249]Consiglio Nazionale delle Ricerche—Istituto dei Sistemi Complessi, Piazzale Aldo Moro 5, I-00185 Roma, Italy
[250]Korea Astronomy and Space Science Institute (KASI), Yuseong-gu, Daejeon 34055, Republic of Korea
[251]Hobart and William Smith Colleges, Geneva, New York 14456, USA
[252]International Institute of Physics, Universidade Federal do Rio Grande do Norte, Natal RN 59078-970, Brazil
[253]Museo Storico della Fisica e Centro Studi e Ricerche "Enrico Fermi", I-00184 Roma, Italy
[254]Dipartimento di Matematica e Fisica, Università degli Studi Roma Tre, I-00146 Roma, Italy
[255]University of Arizona, Tucson, Arizona 85721, USA
[256]Università di Trento, Dipartimento di Matematica, I-38123 Povo, Trento, Italy
[257]University of California, Riverside, Riverside, California 92521, USA
[258]University of Washington, Seattle, Washington 98195, USA
[259]Indian Institute of Technology, Palaj, Gandhinagar, Gujarat 382355, India
[260]Department of Electronic Control Engineering, National Institute of Technology, Nagaoka College, Nagaoka City, Niigata 940-8532, Japan
[261]Departamento de Matemática da Universidade de Aveiro and Centre for Research and Development in Mathematics and Applications, Campus de Santiago, 3810-183 Aveiro, Portugal
[262]Marquette University, Milwaukee, Wisconsin 53233, USA
[263]Faculty of Science, Toho University, Funabashi City, Chiba 274-8510, Japan
[264]Graduate School of Science and Technology, Gunma University, Maebashi, Gunma 371-8510, Japan
[265]Institute for Quantum Studies, Chapman University, Orange, California 92866, USA
[266]Accelerator Laboratory, High Energy Accelerator Research Organization (KEK), Tsukuba City, Ibaraki 305-0801, Japan
[267]Faculty of Information Science and Technology, Osaka Institute of Technology, Hirakata City, Osaka 573-0196, Japan
[268]INAF, Osservatorio Astrofisico di Arcetri, Largo Enrico Fermi 5, I-50125 Firenze, Italy
[269]Indian Institute of Technology Hyderabad, Sangareddy, Khandi, Telangana 502285, India
[270]Indian Institute of Science Education and Research, Pune, Maharashtra 411008, India
[271]Istituto di Astrofisica e Planetologia Spaziali di Roma, Via del Fosso del Cavaliere, 100, 00133 Roma RM, Italy
[272]Department of Space and Astronautical Science, The Graduate University for Advanced Studies (SOKENDAI), Sagamihara City, Kanagawa 252-5210, Japan
[273]Andrews University, Berrien Springs, Michigan 49104, USA
[274]Research Center for Space Science, Advanced Research Laboratories, Tokyo City University, Setagaya, Tokyo 158-0082, Japan
[275]Institute for Cosmic Ray Research (ICRR), Research Center for Cosmic Neutrinos (RCCN), The University of Tokyo, Kashiwa City, Chiba 277-8582, Japan
[276]Department of Physics, Kyoto University, Sakyou-ku, Kyoto City, Kyoto 606-8502, Japan

[277]*Yukawa Institute for Theoretical Physics (YITP), Kyoto University, Sakyou-ku, Kyoto City, Kyoto 606-8502, Japan*
[278]*Dipartimento di Scienze Aziendali—Management and Innovation Systems (DISA-MIS), Università di Salerno, I-84084 Fisciano, Salerno, Italy*
[279]*Van Swinderen Institute for Particle Physics and Gravity, University of Groningen, Nijenborgh 4, 9747 AG Groningen, Netherlands*
[280]*Faculty of Science, Department of Physics, The Chinese University of Hong Kong, Shatin, N.T., Hong Kong*
[281]*Vrije Universiteit Brussel, Pleinlaan 2, 1050 Brussel, Belgium*
[282]*Applied Research Laboratory, High Energy Accelerator Research Organization (KEK), Tsukuba City, Ibaraki 305-0801, Japan*
[283]*Department of Communications Engineering, National Defense Academy of Japan, Yokosuka City, Kanagawa 239-8686, Japan*
[284]*Department of Physics, University of Florida, Gainesville, Florida 32611, USA*
[285]*Department of Information and Management Systems Engineering, Nagaoka University of Technology, Nagaoka City, Niigata 940-2188, Japan*
[286]*Tata Institute of Fundamental Research, Mumbai 400005, India*
[287]*Eindhoven University of Technology, Postbus 513, 5600 MB Eindhoven, Netherlands*
[288]*Department of Physics and Astronomy, Sejong University, Gwangjin-gu, Seoul 143-747, Republic of Korea*
[289]*Concordia University Wisconsin, Mequon, Wisconsin 53097, USA*
[290]*Department of Electrophysics, National Yang Ming Chiao Tung University, Hsinchu 30010, Taiwan*
[291]*Department of Physics, Rikkyo University, Toshima-ku, Tokyo 171-8501, Japan*

[†]Deceased.